INSTITUTE OF PHYSICS PUBLISHING JOURNAL OF OPTICS B: QUANTUM AND SEMICLASSICAL OPTICS
J. Opt. B: Quantum Semiclass. Opt. **6** (2004) S436–S452 PII: S1464-4266(04)71462-7

REVIEW ARTICLE

Modulational instability in a fibre and a fibre Bragg grating

R Ganapathy[1], **K Senthilnathan**[2] **and K Porsezian**[1]

[1] Raman School of Physics, Pondicherry University, R V Nagar, Pondicherry-605 014, India
[2] Department of Physics, Anna University, Chennai-600 025, India

E-mail: ganapathyr@eth.net, senthee2002@yahoo.co.in and ponzsol@yahoo.com

Received 3 November 2003, accepted for publication 14 April 2004
Published 4 May 2004
Online at stacks.iop.org/JOptB/6/S436
DOI: 10.1088/1464-4266/6/5/035

Abstract
In this review article, we study the influence of cross-phase modulation, higher order nonlinear effects such as self-steepening, self-induced Raman scattering and higher order dispersion effects such as third and fourth order dispersion on cross-phase modulational instability for a highly elliptical birefringent optical fibre, and obtain the conditions for the occurrence of cross-phase modulational instability in the normal dispersion regime. In addition, we also consider the pulse propagation through a fibre Bragg grating structure where we investigate the occurrence of modulational instability at the two edges of the photonic bandgap as well as on the upper and lower branches of the dispersion curves.

Keywords: nonlinear fibre, self-phase modulation, cross-phase modulation, birefringence, modulational instability, fibre Bragg grating

1. Introduction

Extensive research has been carried out in the field of pulse propagation in optical fibres [1–6]. On a par with the pulse propagation, continuous wave propagation in optical fibres has also demanded special attention [3, 4]. A continuous wave with a cubic nonlinearity in an anomalous dispersion regime is known to develop instability with respect to small modulations in amplitude or in phase in the presence of noise or any other weak perturbation, called modulational instability (MI) [3, 4, 7–10, 22]. Generally, the perturbation has its origin from quantum noise or from a frequency shifted signal wave [3, 4]. The MI phenomenon was discovered in fluids [12], in nonlinear optics [13] and in plasmas [14]. MI of a light wave in an optical fibre was suggested by Hasegawa and Brinkman [15] as a means to generate a far infrared light source, and since then it has attracted extensive attention for both its fundamental and applied interests [3, 4, 16–22]. As regards applications, MI provides a natural means of generating ultrashort pulses at ultrahigh repetition rates, and is thus potentially useful for the development of high speed optical communication systems in future; hence it has been exploited a great deal in many theoretical and experimental studies for the realization of laser sources adapted to ultrahigh bit-rate optical transmissions [23–25]. The MI phenomenon is accompanied by sideband evolution at a frequency separation from the carrier which is proportional to the square root of the optical pump power [26]. This represents the simplest case of MI in an anomalous dispersion medium with a simple Kerr nonlinearity. When two or more optical waves copropagate through a birefringent optical fibre, they interact with each other through the fibre nonlinearity in such a way that the effective refractive index of a wave depends not only on the intensity of that wave but also on the intensity of other copropagating waves, a phenomenon known as cross-phase modulation (XPM) [1–6, 22]. MI in a birefringent optical fibre can be experimentally observed via two techniques, namely

(i) single-frequency copropagation where two pump waves of identical frequency copropagate with orthogonal polarizations parallel to the two birefringence axes of the fibre [27], and
(ii) two-frequency copropagation, where the two polarized waves copropagate with different frequencies [28].

Drummond *et al* have demonstrated experimentally that MI can occur for the normal dispersion regime by using the single frequency copropagation technique [29]; they pointed out that the appearance of MI in the normal dispersion regime for a highly birefringent fibre is due to the group velocity mismatch (GVM) between the two copropagating waves, and termed the instability as cross-phase MI (XMI) [29]. When breakup of continuous wave and quasi-continuous wave radiates into a train of picosecond and femtosecond pulses in the fibre, higher order nonlinear effects such as self-steepening, self-induced Raman scattering (SRS) and higher order dispersion effects such as third and fourth order dispersion should also be taken into account [2, 30]. The influence of cross-phase modulation (XPM), higher order nonlinear effects such as self-steepening, self-induced Raman scattering (SRS) and higher order dispersion effects such as third and fourth order dispersion on XMI for a highly elliptical birefringent optical fibre is studied in this paper, and conditions for the occurrence of XMI in the normal dispersion regime are obtained.

In recent years, the investigation of pulse propagation in a fibre Bragg grating (FBG) has attracted great attention among researches. For instance, 'Bragg solitons' in a fibre grating were first observed in a 1996 experiment [31]. Thereafter, several innovative theoretical and experimental ideas have been proposed [1, 4]. Hence, for this review article, apart from the studies on MI in fibres which throw light on the conditions required for the generation of ultrashort pulses from a continuous or quasi-continuous wave, we report on studies on MI in an FBG that have also been extensively investigated in recent years, owing to the enormous amount of group velocity dispersion (GVD) provided by the periodic structure in the FBG. Therefore, in the second part, we intend to investigate the phenomenon of MI in a FBG structure.

The outline of the paper is as follows. In section 2, the basic equation is presented. MI conditions for the basic equation are determined in section 3. In section 4 the derivation of the coupled linearized equations for the four side band amplitudes in the two orthogonal linear polarization components of the pump wave is presented, and the MI conditions corresponding to the same are determined and are compared with those in section 3. In section 5, the occurrence of MI is discussed at the edges of the photonic bandgap (PBG) as well as at the normal and anomalous dispersion regimes. Before embarking into the MI discussion, we consider the theoretical model pertaining to the pulse propagation equation in a FBG. We also study the impact of nonlinearity on the PBG, a linear stability analysis of nonlinear coupled mode equations, modulational instability conditions at the anomalous and normal dispersion regimes, and modulational instability conditions at the top and bottom of the photonic band gap, in section 6. In section 7, we discuss the existence of gap solitons derived from the various modulational instability conditions discussed in section 6. The main conclusion of this review article is presented in section 8.

2. Mathematical formulation of the problem

In this section, the case of XPM-induced coupling of two waves having the same frequency but different polarizations is studied. In this regard, the basic equation will have two orthogonal polarization modes, say P_1 and P_2, and hence the nonlinear polarization vector $\mathbf{P}_{\mathrm{NL}}$ has the form [3]

$$\mathbf{P}_{\mathrm{NL}} = \tfrac{1}{2}(\widehat{e}_1 P_1 + \widehat{e}_2 P_2)\exp(-\mathrm{i}\omega_0 t) + \mathrm{c.c.}, \tag{1}$$

where $\widehat{e}_1$ and $\widehat{e}_2$ denote the orthonormal polarization eigenvectors related to the unit vectors $\widehat{x}$ and $\widehat{y}$ oriented along the major and minor axes of the birefringence ellipse, and are given by the expressions [3]

$$\widehat{e}_1 = \frac{\widehat{x} + \mathrm{i}r\widehat{y}}{\sqrt{1+r^2}} \tag{2}$$

and

$$\widehat{e}_2 = \frac{r\widehat{x} - \mathrm{i}\widehat{y}}{\sqrt{1+r^2}}. \tag{3}$$

Here r represents the extent of ellipticity. Considering the slowly varying envelope approximation, the electric field has the form [3]

$$\mathbf{E} = \tfrac{1}{2}(\widehat{e}_1 U + \widehat{e}_2 V)\exp(-\mathrm{i}\omega_0 t) + \mathrm{c.c.}, \tag{4}$$

where U and V are the slowly varying electric field envelopes.

Malomed and Tasgal [32, 33] have derived the equation for the elliptically birefringent fibre pertaining to self-induced Raman scattering for arbitrary ellipticity angle. In this paper, the important steps leading to the derivation of the coupled higher order nonlinear Schrödinger equation (CHNSE) model are outlined below from [32, 33]. Starting from the slowly varying envelope approximation, the final governing equations between the slowly varying electric field envelopes U and V and the two orthogonal polarization modes P_1 and P_2 are given by

$$\begin{aligned} \mathrm{i}U_z &= -\frac{\omega_0^2}{c^2}\left(P_1^{\mathrm{Raman}} + P_1^{\text{non-Raman}}\right) \\ \text{and} \qquad & \qquad (5) \\ \mathrm{i}V_z &= -\frac{\omega_0^2}{c^2}\left(P_2^{\mathrm{Raman}} + P_2^{\text{non-Raman}}\right). \end{aligned}$$

The equations for the Raman effect in an optical fibre in the case of arbitrary ellipticity have been derived in [33] having the form

$$\begin{aligned} \mathbf{P}^{\mathrm{Raman}}(z,T) = \mathbf{E}(z,T)\int_{-\infty}^{+\infty} F_1(T-T')\mathbf{E}(z,T') \\ \times \mathbf{E}(z,T')\,\mathrm{d}T' + \mathbf{E}(z,T)\cdot\int_{-\infty}^{+\infty}\mathbf{E}(z,T')F_2(T-T') \\ \times \mathbf{E}(z,T')\,\mathrm{d}T', \end{aligned} \tag{6}$$

where $\mathbf{E}$ is the electric field and F_1 and F_2 are material functions. Under the slowly varying envelope approximation, as the electric field envelopes U and V and the polarization components P_1 and P_2 are assumed to vary slowly, the rapidly oscillatory out-of-phase terms may be dropped, provided the Raman timescales are much longer than the oscillation period of the electric field. The polarization envelopes—the terms which remain after rapidly oscillating terms are dropped from

equation (6)—are thus given by [33]

$$\begin{aligned}
P_1^{\text{Raman}} &= U(z,T)\int_{-\infty}^{+\infty}[2F_1(T-T') \\
&+ (1+\cos^2\theta)F_2(T-T')]|U(z,T)|^2\,\mathrm{d}T' \\
&+ U(z,T)\int_{-\infty}^{+\infty}[2F_1(T-T') \\
&+ (1+\sin^2\theta)F_2(T-T')]|V(z,T)|^2\,\mathrm{d}T' \\
&+ V(z,T)\int_{-\infty}^{+\infty}(1+\sin^2\theta) \\
&\times F_2(T-T')U(z,T')V^*(z,T')\,\mathrm{d}T' \\
P_2^{\text{Raman}} &= V(z,T)\int_{-\infty}^{+\infty}[2F_1(T-T') \\
&+ (1+\cos^2\theta)F_2(T-T')]|V(z,T)|^2\,\mathrm{d}T' \\
&+ V(z,T)\int_{-\infty}^{+\infty}[2F_1(T-T') \\
&+ (1+\sin^2\theta)F_2(T-T')]|U(z,T)|^2\,\mathrm{d}T' \\
&+ U(z,T)\int_{-\infty}^{+\infty}(1+\sin^2\theta) \\
&\times F_2(T-T')U^*(z,T')V(z,T')\,\mathrm{d}T',
\end{aligned} \tag{7}$$

where the ellipticity angle θ defines the following relations:

$$\widehat{e}_1\cdot\widehat{e}_1 = \widehat{e}_2\cdot\widehat{e}_2 = \cos\theta \qquad \text{and} \qquad \widehat{e}_1\cdot\widehat{e}_2 = \sin\theta. \tag{8}$$

Then, making the connection to the evolution equations, the Raman contribution to the evolution equations takes the form

$$\mathrm{i}U_z|_{\text{Raman}} = P_1^{\text{Raman}} \qquad \text{and} \qquad \mathrm{i}V_z|_{\text{Raman}} = P_2^{\text{Raman}}. \tag{9}$$

In the quasi-instantaneous limit, the functions F_1 and F_2 may be split into an instantaneous part and a quasi-instantaneous part, i.e.

$$F(T) = (F_{\text{inst}})\delta(T) + (F_{\text{quasi-inst}})\delta(T'). \tag{10}$$

The quasi-instantaneous part gives [33]

$$\begin{aligned}
\mathrm{i}U_z|_{\text{Raman}} &= \gamma(U[\varepsilon_3'|U|^2 + \varepsilon_4'|V|^2]_T + \varepsilon_5' V[UV^*]_T), \\
\mathrm{i}V_z|_{\text{Raman}} &= \gamma(V[\varepsilon_4'|U|^2 + \varepsilon_3'|V|^2]_T + \varepsilon_5' U[U^*V]_T),
\end{aligned} \tag{11}$$

where γ is the nonlinearity coefficient. The Raman coefficients ε_3', ε_4' and ε_5' are given by [33]

$$\begin{aligned}
\varepsilon_3' &= \left[2(F_{\text{quasi-inst}})_1 + (1+\cos^2\theta)(F_{\text{quasi-inst}})_2\right], \\
\varepsilon_4' &= \left[2(F_{\text{quasi-inst}})_1 + \sin^2\theta(F_{\text{quasi-inst}})_2\right] \\
\text{and} \qquad \varepsilon_5' &= (1+\sin^2\theta)(F_{\text{quasi-inst}})_2.
\end{aligned} \tag{12}$$

Hence the relation between the three Raman coefficients can be written as

$$\varepsilon_3' = \varepsilon_4' + \frac{2\cos^2\theta}{1+\sin^2\theta}\varepsilon_5'. \tag{13}$$

The contributions due to the non-Raman terms can be derived in the same way as those due to the Raman terms [33] presented in this paper, and also by following a similar procedure for both of the slowly varying electric field envelopes U and V. Furthermore, Menyuk [34] has devised an easy method for deriving the coupled nonlinear Schrödinger equation. Finally, the non-Raman contributions to the evolution equations take the form [33]

$$\begin{aligned}
\mathrm{i}U_z|_{\text{non-Raman}} &= -\Big(\gamma(|U|^2 + B|V|^2)U \\
&+ \mathrm{i}\frac{\gamma}{\omega_0}\left[\left(\varepsilon_1'|U|^2 + \varepsilon_2'|V|^2\right)U\right]_T\Big), \\
\mathrm{i}V_z|_{\text{non-Raman}} &= -\Big(\gamma(B|U|^2 + |V|^2)V \\
&+ \mathrm{i}\frac{\gamma}{\omega_0}\left[\left(\varepsilon_2'|U|^2 + \varepsilon_1'|V|^2\right)V\right]_T\Big),
\end{aligned} \tag{14}$$

where the terms in the square brackets denote the effect due to self-steepening [33]. ε_1' and ε_2' are constants and are the coefficients of the self-steepening terms. The cross-phase modulation coefficient B is a function of ellipticity, and is given by [34]

$$B = \frac{2+2\sin^2\theta}{2+\cos^2\theta}. \tag{15}$$

This gives $B = \frac{2}{3}$ for linear ellipticity $\theta = 0$; $B = 2$ for circular ellipticity $\theta = 90°$, and $B = 1$ for the ideal birefringence case, for which $\theta \approx 35.3°$. Finally, the linear contributions to the evolution equations yield

$$\begin{aligned}
\mathrm{i}U_z|_{\text{Linear}} &= \left(-\mathrm{i}\frac{\delta}{2}U_T + \frac{\beta_2}{2}U_{TT} + \mathrm{i}\frac{\beta_3}{6}U_{TTT} + \frac{\beta_4}{24}U_{TTTT}\right), \\
\mathrm{i}V_z|_{\text{Linear}} &= \left(\mathrm{i}\frac{\delta}{2}V_T + \frac{\beta_2}{2}V_{TT} + \mathrm{i}\frac{\beta_3}{6}V_{TTT} + \frac{\beta_4}{24}V_{TTTT}\right),
\end{aligned} \tag{16}$$

where β_2, β_3 and β_4 are the second, third and fourth order dispersion coefficients, respectively. Considering both these higher order dispersion and nonlinear effects, the coupled higher order nonlinear Schrödinger equation (CHNSE) model [30, 32, 33] with the addition of self-steepening, SRS, third and fourth order dispersion effects is given by

$$\begin{aligned}
&\mathrm{i}\left(U_z + \frac{\delta}{2}U_T\right) - \frac{\beta_2}{2}U_{TT} + \gamma(|U|^2 + B|V|^2)U \\
&- \mathrm{i}\frac{\beta_3}{6}U_{TTT} - \frac{\beta_4}{24}U_{TTTT} + \mathrm{i}\frac{\gamma}{\omega_0}\left[\left(\varepsilon_1'|U|^2 + \varepsilon_2'|V|^2\right)U\right]_T \\
&- \gamma\left(U\left[\varepsilon_3'|U|^2 + \varepsilon_4'|V|^2\right]_T\right. \\
&\left.+ \varepsilon_5' V[UV^*]_T\right) = 0, \\
&\mathrm{i}\left(V_z - \frac{\delta}{2}V_T\right) - \frac{\beta_2}{2}V_{TT} + \gamma(B|U|^2 + |V|^2)V \\
&- \mathrm{i}\frac{\beta_3}{6}V_{TTT} - \frac{\beta_4}{24}V_{TTTT} + \mathrm{i}\frac{\gamma}{\omega_0}\left[\left(\varepsilon_2'|U|^2 + \varepsilon_1'|V|^2\right)V\right]_T \\
&- \gamma\left(V\left[\varepsilon_4'|U|^2 + \varepsilon_3'|V|^2\right]_T\right. \\
&\left.+ \varepsilon_5' U[U^*V]_T\right) = 0,
\end{aligned} \tag{17}$$

where z is the longitudinal distance, and $T = t - \frac{z}{v_g}$ is the retarded time.

In the dimensionless form, the above equation becomes

$$\begin{aligned}
&\mathrm{i}(u'_\varsigma + \Delta u'_\tau) - S_1 u'_{\tau\tau} + \left[|u'|^2 + B|v'|^2\right]u' - \mathrm{i}S_2 u'_{\tau\tau\tau} \\
&\quad - S_3 u'_{\tau\tau\tau\tau} + \mathrm{i}\left[\left(\varepsilon_1|u'|^2 + \varepsilon_2|v'|^2\right)u'\right]_\tau \\
&\quad - \left(u'\left[\varepsilon_3|u'|^2 + \varepsilon_4|v'|^2\right]_\tau + \varepsilon_5 v'[u'v'^*]_\tau\right) = 0, \\
&\mathrm{i}(v'_\varsigma - \Delta v'_\tau) - S_1 v'_{\tau\tau} + \left[B|u'|^2 + |v'|^2\right]v' - \mathrm{i}S_2 v'_{\tau\tau\tau} \\
&\quad - S_3 v'_{\tau\tau\tau\tau} + \mathrm{i}[(\varepsilon_2|u'|^2 + \varepsilon_1|v'|^2)v']_\tau \\
&\quad - \left(v'\left[\varepsilon_4|u'|^2 + \varepsilon_3|v'|^2\right]_\tau + \varepsilon_5 u'[u'^* v']_\tau\right) = 0,
\end{aligned} \tag{18}$$

where

$$\begin{aligned}
&\varsigma = \frac{z}{T_0^2}|\beta_2|; \qquad \tau = \frac{T}{T_0}; \qquad \Delta = \frac{T_0\delta}{2|\beta_2|}; \\
&S_1 = \frac{s_1}{2}; \qquad S_2 = \frac{s_2|\beta_3|}{6T_0|\beta_2|}; \qquad S_3 = \frac{s_3|\beta_4|}{24T_0^2|\beta_2|}; \\
&U = \sqrt{\frac{|\beta_2|}{\gamma T_0^2}}u'; \qquad V = \sqrt{\frac{|\beta_2|}{\gamma T_0^2}}v'; \qquad \varepsilon_1 = \frac{\varepsilon'_1}{\omega_0 T_0}; \\
&\varepsilon_2 = \frac{\varepsilon'_2}{\omega_0 T_0}; \qquad \varepsilon_3 = \frac{\varepsilon'_3}{T_0}; \qquad \varepsilon_4 = \frac{\varepsilon'_4}{T_0}; \\
&\varepsilon_5 = \frac{\varepsilon'_5}{T_0},
\end{aligned}$$

where T_0 is an arbitrary timescale and $s_i = \pm 1$ $(i = 1, 2, 3)$.

Cavalcanti *et al* have theoretically analysed MI in the region of minimum group velocity dispersion of single-mode fibres by means of an extended nonlinear Schrödinger equation, taking into account fourth order dispersive effects [35]. They have demonstrated that the fourth order dispersive term dominates the critical MI frequency when the second order dispersion approaches its minimum value at the zero dispersion wavelength. Furthermore, they have demonstrated experimentally the generation of a train of femtosecond pulses having period of modulation of the order of 500 fs and with repetition rates given by the modulation frequency. As a follow-up, in the region of minimum group velocity dispersion, Akhmediev *et al* have discussed the significance of the fourth order dispersion effect, which predominates over other higher order effects, in the context of solitary waves with radiationless oscillating tails [36, 37], and have analysed the stability criteria for stationary bound states of solitary waves of the order of 500 fs. In this review article, as the first case, we intend to investigate, in the region of minimum group velocity dispersion, the XMI conditions required for the generation of ultrashort pulses having period of modulation of the order of 500 fs. As the second case, for $|\beta_2|$ having a sufficiently large value, we would like to determine the XMI conditions required for the generation of ultrashort pulses below 500 fs where the influence of SRS and self-steepening should be considered [30, 38], and where the higher order dispersion effects can safely be neglected as their parameter values are much too small when compared to the group velocity dispersion term.

3. Stability analysis and modulational instability conditions

In the case of continuous wave or quasi-continuous wave radiations, the orthogonally polarized amplitudes u' and v' are independent of τ at the input end of the fibre at $\zeta = 0$. Considering the case for a linearly polarized pump oriented at an arbitrary angle with respect to either the slow or the fast axis of the birefringent fibre, and assuming that both $u'(\zeta, \tau)$ and $v'(\zeta, \tau)$ remain time independent during propagation inside the fibre, equation (18) admits steady-state solutions of the form [3]

$$\begin{aligned}
u' &= \sqrt{P_1}\exp(\mathrm{i}\zeta(P_1 + BP_2)), \\
v' &= \sqrt{P_2}\exp(\mathrm{i}\zeta(P_2 + BP_1)),
\end{aligned} \tag{19}$$

where $P_{1,2}$ are proportional to input powers along the principal axes. These steady-state solutions imply that light propagates through the birefringent fibre unchanged except for acquiring a power-dependent phase shift. The stability of the steady-state solution is examined by looking into the system in the presence of small amplitude perturbations $u(\zeta, \tau)$ and $v(\zeta, \tau)$ given by

$$\begin{aligned}
u' &= (\sqrt{P_1} + u)\exp(\mathrm{i}\zeta(P_1 + BP_2)), \\
v' &= (\sqrt{P_2} + v)\exp(\mathrm{i}\zeta(P_2 + BP_1)).
\end{aligned} \tag{20}$$

On substituting equation (20) into (18) and on linearizing in $u(\zeta, \tau)$ and $v(\zeta, \tau)$, the following linearized equations in $u(\zeta, \tau)$ and $v(\zeta, \tau)$ are obtained:

$$\begin{aligned}
&\mathrm{i}(u_\varsigma + \Delta u_\tau) - S_1 u_{\tau\tau} + \left(P_1(u + u^*)\right. \\
&\quad \left. + B\sqrt{P_1P_2}(v + v^*)\right) - \mathrm{i}S_2 u_{\tau\tau\tau} - S_3 u_{\tau\tau\tau\tau} \\
&\quad + \mathrm{i}\left(\varepsilon_1 P_1[u^* + 2u]_\tau + \varepsilon_2\left[P_2 u + \sqrt{P_1P_2}(v + v^*)\right]_\tau\right) \\
&\quad - \left(\varepsilon_3 P_1[u + u^*]_\tau + \varepsilon_4\sqrt{P_1P_2}[v + v^*]_\tau\right. \\
&\quad \left. + \varepsilon_5\left[P_2 u + \sqrt{P_1P_2}v^*\right]_\tau\right) = 0, \\
&\mathrm{i}(v_\varsigma - \Delta v_\tau) - S_1 v_{\tau\tau} + \left(B\sqrt{P_1P_2}(u + u^*) + P_2(v + v^*)\right) \\
&\quad - \mathrm{i}S_2 v_{\tau\tau\tau} - S_3 v_{\tau\tau\tau\tau} + \mathrm{i}\left(\varepsilon_1 P_2[v^* + 2v]_\tau\right. \\
&\quad \left. + \varepsilon_2\left[P_1 v + \sqrt{P_1P_2}(u + u^*)\right]_\tau\right) \\
&\quad - \left(\varepsilon_3 P_2[v + v^*]_\tau + \varepsilon_4\sqrt{P_1P_2}[u + u^*]_\tau\right. \\
&\quad \left. + \varepsilon_5\left[\sqrt{P_1P_2}u^* + P_1 v\right]_\tau\right) = 0.
\end{aligned} \tag{21}$$

The Fourier transforms of $u(\zeta, \tau)$ and $v(\zeta, \tau)$ are

$$\begin{aligned}
A_1(\zeta, \omega) &= \frac{1}{\sqrt{2\pi}}\int_{-\infty}^{+\infty} u(\zeta, \tau)\exp(\mathrm{i}\omega\tau)\,\mathrm{d}\tau, \\
A_2(\zeta, \omega) &= \frac{1}{\sqrt{2\pi}}\int_{-\infty}^{+\infty} v(\zeta, \tau)\exp(\mathrm{i}\omega\tau)\,\mathrm{d}\tau,
\end{aligned} \tag{22}$$

which yield the inverse Fourier transforms

$$\begin{aligned}
u(\zeta, \tau) &= \frac{1}{\sqrt{2\pi}}\int_{-\infty}^{+\infty} A_1(\zeta, \omega)\exp(-\mathrm{i}\omega\tau)\,\mathrm{d}\omega \\
&= \frac{1}{\sqrt{2\pi}}\int_{-\infty}^{+\infty} A_1(\zeta, -\omega)\exp(\mathrm{i}\omega\tau)\,\mathrm{d}\omega,
\end{aligned} \tag{23}$$

$$\begin{aligned}
v(\zeta, \tau) &= \frac{1}{\sqrt{2\pi}}\int_{-\infty}^{+\infty} A_2(\zeta, \omega)\exp(-\mathrm{i}\omega\tau)\,\mathrm{d}\omega \\
&= \frac{1}{\sqrt{2\pi}}\int_{-\infty}^{+\infty} A_2(\zeta, -\omega)\exp(\mathrm{i}\omega\tau)\,\mathrm{d}\omega.
\end{aligned} \tag{24}$$

On substituting equations (23) and (24) into (21) and on considering the relation given by

$$A_i^{\dagger}(\zeta,\omega) = A_i^{*}(\zeta,-\omega), \tag{25}$$

where $i = 1, 2$, equation (23) gets transformed to the following set of equations:

$$\frac{1}{\sqrt{2\pi}}\int_{-\infty}^{+\infty}\left(\mathrm{i}\frac{\partial A_1}{\partial\zeta} + N_{11}A_1 + N_{12}A_1^{\dagger} + N_{13}A_2 + N_{14}A_2^{\dagger}\right) \times \exp(-\mathrm{i}\omega\tau)\,\mathrm{d}\omega = 0 \tag{26}$$

and

$$\frac{1}{\sqrt{2\pi}}\int_{-\infty}^{+\infty}\left(\mathrm{i}\frac{\partial A_2}{\partial\zeta} + N_{21}A_1 + N_{22}A_1^{\dagger} + N_{23}A_2 + N_{24}A_2^{\dagger}\right) \times \exp(-\mathrm{i}\omega\tau)\,\mathrm{d}\omega = 0, \tag{27}$$

where

$$\begin{aligned}
N_{11} &= \Delta\omega + S_2\omega^3 + P_1 + S_1\omega^2 + 2\varepsilon_1 P_1\omega + \varepsilon_2 P_2\omega + \mathrm{i}\varepsilon_3 P_1\omega \\
&\quad + \mathrm{i}\varepsilon_5 P_2\omega - S_3\omega^4, \\
N_{12} &= P_1 + \varepsilon_1 P_1\omega + \mathrm{i}\varepsilon_3 P_1\omega, \\
N_{13} &= B\sqrt{P_1P_2} + \mathrm{i}\varepsilon_4\sqrt{P_1P_2}\omega + \varepsilon_2\sqrt{P_1P_2}\omega, \\
N_{14} &= B\sqrt{P_1P_2} + \varepsilon_2\sqrt{P_1P_2}\omega + \mathrm{i}\varepsilon_4\sqrt{P_1P_2}\omega + \mathrm{i}\varepsilon_5\sqrt{P_1P_2}\omega, \\
N_{21} &= N_{13}, \\
N_{22} &= N_{14}, \\
N_{23} &= -\Delta\omega + S_2\omega^3 + P_2 + S_1\omega^2 + 2\varepsilon_1 P_2\omega + \varepsilon_2 P_1\omega \\
&\quad + \mathrm{i}\varepsilon_3 P_2\omega + \mathrm{i}\varepsilon_5 P_1\omega - S_3\omega^4, \\
N_{24} &= P_2 + \varepsilon_1 P_2\omega + \mathrm{i}\varepsilon_3 P_2\omega.
\end{aligned}$$

On taking the complex conjugate of equation (21) and proceeding as above, one more set of equations is obtained:

$$\frac{1}{\sqrt{2\pi}}\int_{-\infty}^{+\infty}\left(\mathrm{i}\frac{\partial A_1^{\dagger}}{\partial\zeta} + N_{31}A_1 + N_{32}A_1^{\dagger} + N_{33}A_2 + N_{34}A_2^{\dagger}\right) \times \exp(-\mathrm{i}\omega\tau)\,\mathrm{d}\omega = 0 \tag{28}$$

and

$$\frac{1}{\sqrt{2\pi}}\int_{-\infty}^{+\infty}\left(\mathrm{i}\frac{\partial A_2^{\dagger}}{\partial\zeta} + N_{41}A_1 + N_{42}A_1^{\dagger} + N_{43}A_2 + N_{44}A_2^{\dagger}\right) \times \exp(-\mathrm{i}\omega\tau)\,\mathrm{d}\omega = 0, \tag{29}$$

where

$$\begin{aligned}
N_{31} &= -P_1 + \varepsilon_1 P_1\omega - \mathrm{i}\varepsilon_3 P_1\omega, \\
N_{32} &= \Delta\omega + S_2\omega^3 - P_1 - S_1\omega^2 + 2\varepsilon_1 P_1\omega + \varepsilon_2 P_2\omega \\
&\quad - \mathrm{i}\varepsilon_3 P_1\omega - \mathrm{i}\varepsilon_5 P_2\omega + S_3\omega^4, \\
N_{33} &= -B\sqrt{P_1P_2} + \varepsilon_2\sqrt{P_1P_2}\omega - \mathrm{i}\varepsilon_4\sqrt{P_1P_2}\omega \\
&\quad - \mathrm{i}\varepsilon_5\sqrt{P_1P_2}\omega, \\
N_{34} &= -B\sqrt{P_1P_2} - \mathrm{i}\varepsilon_4\sqrt{P_1P_2}\omega + \varepsilon_2\sqrt{P_1P_2}\omega, \\
N_{41} &= N_{33}, \\
N_{42} &= N_{34}, \\
N_{43} &= -P_1 + \varepsilon_1 P_2\omega - \mathrm{i}\varepsilon_3 P_2\omega, \\
N_{44} &= -\Delta\omega + S_2\omega^3 - P_2 - S_1\omega^2 + 2\varepsilon_1 P_2\omega + \varepsilon_2 P_1\omega \\
&\quad - \mathrm{i}\varepsilon_3 P_2\omega - \mathrm{i}\varepsilon_5 P_1\omega + S_3\omega^4.
\end{aligned}$$

On considering the case when the linearly polarized pump is oriented at 45° with respect to both the axes such that power is equally distributed along both axes, i.e., $P_1 = P_2 = P$ with the total input power being $2P$, and on equating the integrands in equations (26)–(29) equal to zero and after some manipulation, four linearized equations in terms of $A_1 + A_1^{\dagger}$, $A_1 - A_1^{\dagger}$, $A_2 + A_2^{\dagger}$ and $A_2 - A_2^{\dagger}$ are obtained which are of the form

$$\begin{aligned}
\mathrm{i}\frac{\partial(A_1 + A_1^{\dagger})}{\partial\zeta} &= M_{11}(A_1 + A_1^{\dagger}) + M_{12}(A_1 - A_1^{\dagger}) \\
&\quad + M_{13}(A_2 + A_2^{\dagger}) + M_{14}(A_2 - A_2^{\dagger}), \\
\mathrm{i}\frac{\partial(A_1 - A_1^{\dagger})}{\partial\zeta} &= M_{21}(A_1 + A_1^{\dagger}) + M_{22}(A_1 - A_1^{\dagger}) \\
&\quad + M_{23}(A_2 + A_2^{\dagger}) + M_{24}(A_2 - A_2^{\dagger}), \\
\mathrm{i}\frac{\partial(A_2 + A_2^{\dagger})}{\partial\zeta} &= M_{31}(A_1 + A_1^{\dagger}) + M_{32}(A_1 - A_1^{\dagger}) \\
&\quad + M_{33}(A_2 + A_2^{\dagger}) + M_{34}(A_2 - A_2^{\dagger}), \\
\mathrm{i}\frac{\partial(A_2 - A_2^{\dagger})}{\partial\zeta} &= M_{41}(A_1 + A_1^{\dagger}) + M_{42}(A_1 - A_1^{\dagger}) \\
&\quad + M_{43}(A_2 + A_2^{\dagger}) + M_{44}(A_2 - A_2^{\dagger}),
\end{aligned}$$

where

$$M_{11} = \Delta\omega + S_2\omega^3 + P\omega(3\varepsilon_1 + \varepsilon_2),$$

$$M_{12} = S_1\omega^2 - S_3\omega^4 + \mathrm{i}\varepsilon_5 P\omega,$$

$$M_{13} = 2\varepsilon_2 P\omega,$$

$$M_{14} = -\mathrm{i}\varepsilon_5 P\omega,$$

$$M_{21} = S_1\omega^2 - S_3\omega^4 + 2P + \mathrm{i}P\omega(2\varepsilon_3 + \varepsilon_5),$$

$$M_{22} = \Delta\omega + S_2\omega^3 + P\omega(\varepsilon_1 + \varepsilon_2),$$

$$M_{23} = 2BP + \mathrm{i}P\omega(2\varepsilon_4 + \varepsilon_5),$$

$$M_{24} = 0,$$

$$M_{31} = 2\varepsilon_2 P\omega,$$

$$M_{32} = -\mathrm{i}\varepsilon_5 P\omega,$$

$$M_{33} = -\Delta\omega + S_2\omega^3 + P\omega(3\varepsilon_1 + \varepsilon_2),$$

$$M_{34} = M_{12},$$

$$M_{41} = 2BP + \mathrm{i}P\omega(2\varepsilon_4 + \varepsilon_5),$$

$$M_{42} = 0,$$

$$M_{43} = M_{21},$$

$$M_{44} = -\Delta\omega + S_2\omega^3 + P\omega(\varepsilon_1 + \varepsilon_2).$$

These equations can be brought into the following matrix form:

$$\mathrm{i}\frac{\partial\mathbf{A}(\varsigma,\omega)}{\partial\zeta} = -\mathbf{M}(\omega)\mathbf{A}(\varsigma,\omega) \tag{30}$$

where

$$\mathbf{A}(\varsigma,\omega)=\begin{pmatrix}A_1+A_1^{\dagger}\\ A_1-A_1^{\dagger}\\ A_2+A_2^{\dagger}\\ A_2-A_2^{\dagger}\end{pmatrix} \tag{31}$$

and

$$\mathbf{M}(\omega)=\begin{pmatrix}M_{11} & M_{12} & M_{13} & M_{14}\\ M_{21} & M_{22} & M_{23} & 0\\ M_{31} & M_{32} & M_{33} & M_{34}\\ M_{41} & 0 & M_{43} & M_{44}\end{pmatrix}. \tag{32}$$

The eigenvalue equation is given by

$$|\mathbf{M}(\omega)-k\mathbf{I}|=0, \tag{33}$$

where $\mathbf{I}$ is the identity matrix. From equation (33), a dispersion relation in k is obtained which is a fourth order polynomial equation. As is well known, MI occurs when there is an exponential growth in the amplitude of the perturbed wave which implies the existence of a nonvanishing imaginary part in the complex eigenvalue k [3, 22]. The MI phenomenon is measured by a gain given by $G=|\mathrm{Im}\,k|$ where $\mathrm{Im}\,k$ denotes the imaginary part of k. The gain parameter G throws light on the MI conditions for the three different scenarios of pulse propagation mentioned in section 2. The results obtained for the three different cases are discussed below.

3.1. The MI condition governing the generation of ultrashort pulses of the order of 500 fs in the region of minimum group velocity dispersion

This scenario has been experimentally studied by Cavalacanti *et al* for the scalar nonlinear Schrödinger equation [35]. The case when the linearly polarized pump is oriented at 45° with respect to both the axes such that equal power is distributed along each axis, i.e., $P_1=P_2=P$ with the total input power being $2P$, is considered. From equation (33), the dispersion relation between k and ω is obtained, which is of the form

$$k^4-4S_2\omega^3k^3-2\omega^2L_1k^2+4S_2\omega^5L_2k+\omega^4L_3=0, \tag{34}$$

where

$$L_1=\Delta^2+\omega^2(S_1^2-3S_2^2\omega^2+S_3^2\omega^4)-S_1(2S_3\omega^4-P),$$
$$L_2=\Delta^2+\omega^2(S_1^2-S_2^2\omega^2+S_3^2\omega^4-S_3P)-S_1(2S_3\omega^4-P)$$

and

$$L_3=\Delta^4+\omega^4(-S_2^2\omega^2+(S_1-S_3\omega^2)^2)^2+(1-B^2)(S_1-S_3\omega^2)^2P^2+2\omega^2(S_1-S_3\omega^2)\left(-S_2^2\omega^2+(S_1-S_3\omega^2)^2\right)P-2\Delta^2\left(\omega^2(S_1^2+S_2^2\omega^2+S_3^2\omega^4-S_3P)-S_1(2S_3\omega^4-P)\right).$$

$S_1=-\frac{1}{2}$ portrays the case of MI in the anomalous dispersion regime which has been discussed in detail in [3, 29]. The normal dispersion regime denoted by $S_1=\frac{1}{2}$ is now analysed. In this case, the complex eigenvalue k obtained from the dispersion relation given by equation (34) has the form

$$k=S_2\omega^3\pm\omega\sqrt{L_4\pm2\sqrt{L_5}}, \tag{35}$$

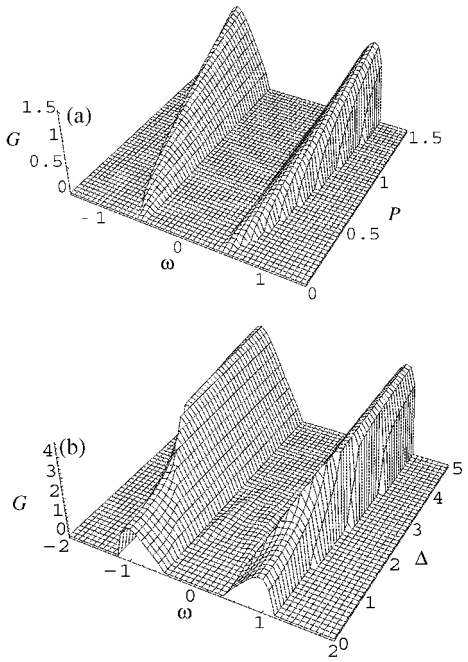

Figure 1. Surface plots of the gain spectrum G for case (i) when $|\beta_2|=0.000\,05$ ps^2 K^{-1} m^{-1}, $|\beta_3|=0.54\times10^{-3}$ ps^3 K^{-1} m^{-1} and $|\beta_4|=7.0\times10^{-4}$ ps^4 K^{-1} m^{-1}: (a) gain spectrum as a function of frequency detuning ω and input power P for $\Delta=3.925$, $S_1=0.5$, $S_2=2.6087\times10^{-6}$ and $S_3=1.690\,82\times10^{-6}$; (b) gain spectrum as a function of frequency detuning ω and group velocity mismatch Δ for $P=5.0$ and having the same values for the rest of the parameters as in (a).

where

$$L_4=\Delta^2+(S_1-S_3\omega^2)(S_1\omega^2-S_3\omega^4+2P),$$
$$L_5=(S_1-S_3\omega^2)\left(B^2(S_1-S_3\omega^2)P^2+\Delta^2(S_1\omega^2-S_3\omega^4+2P)\right).$$

Equation (35) is found to possess a non-zero imaginary part only for the case given by

$$k=S_2\omega^3\pm\omega\sqrt{L_4-2\sqrt{L_5}}. \tag{36}$$

Hence, from the above equation, the condition for instability to occur is determined, which is given by $L_4^2<4L_5$. From equation (36) it is clear that the instability condition is not affected irrespective of the presence or absence of S_2, the dimensionless third order dispersion coefficient. Figure 1(a) shows the graphical relation between the frequency detuning ω, input power P and gain G for $B=\frac{2}{3}$ which depicts linear birefringence, $\Delta=5.416\,67\times10^6$, $S_1=0.5$, $S_2=3.6$ and $S_3=2.3333$. This corresponds to the case when $|\beta_2|=0.000\,05$ ps^2 K^{-1} m^{-1}, $|\beta_3|=0.54\times10^{-3}$ ps^3 K^{-1} m^{-1} and $|\beta_4|=7.0\times10^{-4}$ ps^4 K^{-1} m^{-1}. From figure 1(a), it is evident that as $|\beta_2|$ is close to zero, we obtain the usual MI gain spectrum as in the anomalous dispersion regime case. In figure 1(b), which shows the graphical relation between gain G, group velocity mismatch Δ and frequency detuning ω for $P=5.0$ and with the other parameters having the same values as in figure 1(a), the instability occurs for all values of group velocity mismatch. As is well known, the XPM coupling factor B depends on the ellipticity angle θ, and

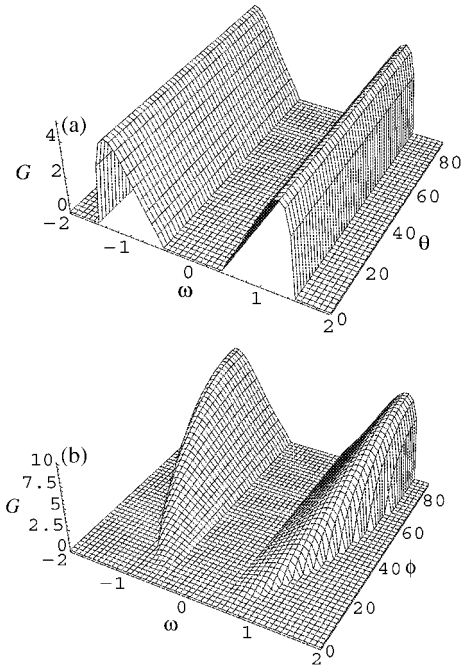

Figure 2. Surface plots of the gain spectrum G for case (i): (a) gain spectrum as a function of frequency detuning ω and ellipticity angle θ for the same values as in figure 1; (b) gain spectrum as a function of frequency detuning ω and polarization angle ϕ for the same values as in figure 1.

can vary from $\frac{2}{3}$ to 2 for values of θ in the range 0–$\frac{\pi}{2}$ [1–3]. $\theta = 0$ corresponds to linear birefringence for which $B = \frac{2}{3}$, and $\theta = \frac{\pi}{2}$ corresponds to circular birefringence for which $B = 2$ [1–4]. For $\theta \approx 35°$, $B = 1.0$, which corresponds to the ideal birefringence case where the self-and cross-phase coupling terms are identical [26]. Figure 2(a) shows the variation of gain G with respect to the frequency detuning ω and the ellipticity angle θ for $P = 5.0$. In this case, the peaks of the gain curve have the same value for all values of θ. To study the effect of variations in the pump polarization wherein the pump power is not distributed equally along both the axes, the pump powers in terms of the polarization angle ϕ can be written in the form $P_1 = 2P\cos^2(\phi)$ and $P_2 = 2P\sin^2(\phi)$ such that the total pump power is always equal to $2P$. On substituting these into the eigenvalue equation (33), the MI condition is determined numerically. Figure 2(b) depicts the surface plot of the gain spectrum as a function of the frequency detuning ω and the polarization angle ϕ. Here the peaks of the sideband lobes are found to increase with increase in polarization angle.

3.2. The MI condition governing the generation of ultrashort pulses in the femtosecond region below 500 fs

It is not possible to neglect the influence of SRS and self-steepening on the MI in this regime as it is typically larger than other perturbations and, unlike dispersion, the Raman effect is nonconservative and can thus cause a permanent redistribution of the pulses' internal energy [33]. For the same values of the dispersion parameters as considered in figure 1(a) and with $\Delta = 1.963$, $S_1 = 0.5$, $S_2 = 0$, $S_3 = 0$, $\varepsilon_1 = \varepsilon_2 = 4.0 \times 10^{-6}$, $\varepsilon_3 = 0.03$, $\varepsilon_4 = \varepsilon_5 = 0.01$, the XMI condition is determined by numerically evaluating

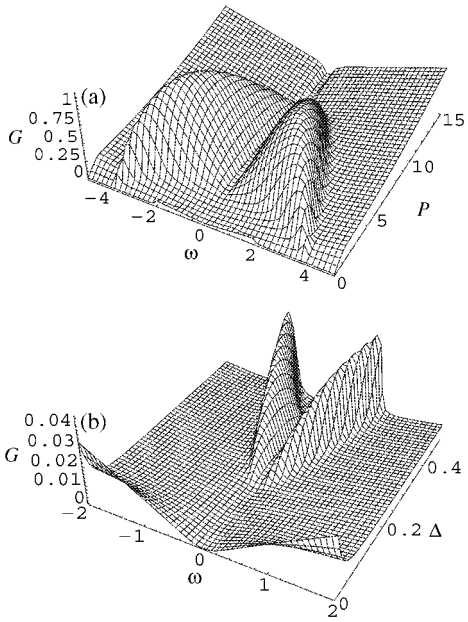

Figure 3. Surface plots of the gain spectrum G for case (ii) with $|\beta_2| = 69.0\ \mathrm{ps^2\ K^{-1}\ m^{-1}}$, $S_1 = 0.5$, $\varepsilon_1 = \varepsilon_2 = 4.0 \times 10^{-6}$, $\varepsilon_3 = 0.03$, $\varepsilon_4 = \varepsilon_5 = 0.01$: (a) gain spectrum as a function of frequency detuning ω and input power P for $\Delta = 1.963$; (b) gain spectrum as a function of frequency detuning ω and group velocity mismatch Δ for $P = 0.1$.

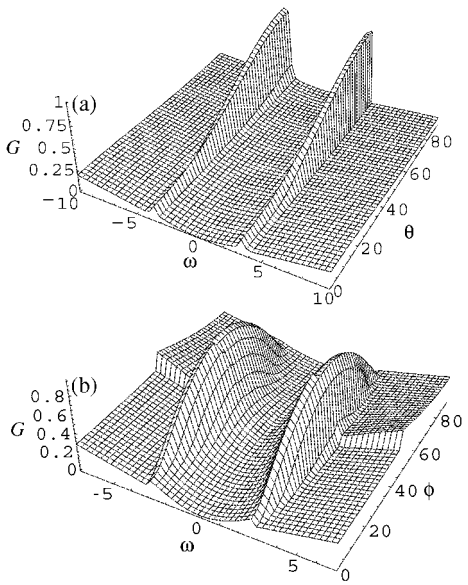

Figure 4. Surface plots of the gain spectrum G for case (ii) with $\Delta = 1.963$ and $P = 0.1$. The rest of the parameters have the same values as in figure 3: (a) gain spectrum as a function of frequency detuning ω and ellipticity angle θ; (b) gain spectrum as a function of frequency detuning ω and polarization angle ϕ.

the eigenvalue equation (33) when the linearly polarized pump is polarized equally with respect to either axis. The corresponding gain spectrum as a function of frequency detuning ω and input power P is portrayed in figure 3(a). From figure 3(a), it is evident that for comparatively low values of ω, the gain spectrum is dominated more by XPM and GVD effects, with the result that in that specific region, as the pump power is increased, the peaks of the gain curve move closer to

the zero detuning frequency with the peak position changing relatively slowly when compared to the increase in the gain band width.

By suitably adjusting the various parameters, it can be inferred from figures 3 and 4 that while self-steepening reduces the maximum value of the gain spectrum, SRS enhances the region of MI. One effect dominates over the other depending on the values of the various parameters considered in this paper. In most cases the SRS dominates over the self-steepening effect. As a result, for comparatively higher values of ω and with increasing power, the SRS effect becomes predominant, with the result that the gain spectrum increases linearly with ω. In a nutshell, the effect of SRS widens the region of MI whereas the effect of self-steepening tries to reduce the maximum gain, which is evident from figure 3(a). A marked difference between the findings obtained in case (ii) and that obtained in [29] is due to the influence of the SRS term in the former, where the gain spectrum increases linearly with ω, which is completely absent in the latter. Figures 3(b), 4(a) and (b), which portray the frequency dependent gain as functions of Δ, θ and ϕ respectively for an input power $P = 0.1$, bring forth similar effects of SRS on MI as portrayed in figure 3(a), with the result that the gain parameter has non-zero values everywhere except for the zero detuning frequency where the gain parameter vanishes.

4. The MI phenomenon in terms of Stokes and anti-Stokes side band amplitudes

The regions of instability may also be understood as arising from a process in which the group velocity dispersion of the down-shifted sideband polarized on the slow axis and the up-shifted sideband on the fast axis is balanced by the group velocity mismatch. This can be verified by assuming for perturbation a modulation ansatz with wavenumber k and frequency ω of the form

$$\begin{aligned} u(\varsigma,\tau) &= u_{\mathrm{s}}(\varsigma)\exp(\mathrm{i}\omega\tau) + u_{\mathrm{a}}(\varsigma)\exp(-\mathrm{i}\omega\tau),\\ v(\varsigma,\tau) &= v_{\mathrm{s}}(\varsigma)\exp(\mathrm{i}\omega\tau) + v_{\mathrm{a}}(\varsigma)\exp(-\mathrm{i}\omega\tau), \end{aligned} \tag{37}$$

where u_{s} and u_{a} can be regarded, respectively, as the measures of the amplitudes of the Stokes and anti-Stokes sidebands for the slow axis, whereas v_{s} and v_{a} represent those for the fast axis. On substituting the above expressions into equation (18) and on linearizing with respect to $u_{\mathrm{s}}, u_{\mathrm{a}}^*, v_{\mathrm{s}}$ and v_{a}^*, a set of coupled linear ordinary differential equations in terms of the perturbing fields $u_{\mathrm{s}}, u_{\mathrm{a}}^*, v_{\mathrm{s}}$ and v_{a}^* is obtained which can be written in the form of a matrix equation given by

$$-\mathrm{i}\frac{\mathrm{d}\mathbf{X}(\varsigma)}{\mathrm{d}\varsigma} = \mathbf{L}\mathbf{X}(\varsigma), \tag{38}$$

where the column matrix $\mathbf{X}(\varsigma) = \begin{pmatrix} u_{\mathrm{s}} \\ u_{\mathrm{a}}^* \\ v_{\mathrm{s}} \\ v_{\mathrm{a}}^* \end{pmatrix}$ and

$$\mathbf{L} = \begin{pmatrix} L_{11} & L_{12} & L_{13} & L_{14} \\ L_{21} & L_{22} & L_{23} & L_{24} \\ L_{31} & L_{32} & L_{33} & L_{34} \\ L_{41} & L_{42} & L_{43} & L_{44} \end{pmatrix}, \tag{39}$$

where the elements of $\mathbf{L}$ take the form

$$\begin{aligned}
L_{11} &= P_1 - \Delta\omega + S_1\omega^2 - S_3\omega^4 - S_2\omega^3 \\
&\quad - \omega(2\varepsilon_1 P_1 + \varepsilon_2 P_2) - \mathrm{i}\omega(\varepsilon_3 P_1 + \varepsilon_5 P_2);\\
L_{12} &= P_1(1 - \varepsilon_1\omega - \mathrm{i}\varepsilon_3\omega);\\
L_{13} &= \sqrt{P_1 P_2}(B - \varepsilon_2\omega - \mathrm{i}\varepsilon_4\omega);\\
L_{14} &= \sqrt{P_1 P_2}(B - \varepsilon_2\omega - \mathrm{i}\varepsilon_4\omega - \mathrm{i}\varepsilon_5\omega);\\
L_{21} &= P_1(-1 - \varepsilon_1\omega + \mathrm{i}\varepsilon_3\omega);\\
L_{22} &= -P_1 - \Delta\omega - S_1\omega^2 + S_3\omega^4 - S_2\omega^3 \\
&\quad - \omega(2\varepsilon_1 P_1 + \varepsilon_2 P_2) + \mathrm{i}\omega(2\varepsilon_3 P_1 + \varepsilon_5 P_2);\\
L_{23} &= \sqrt{P_1 P_2}(-B - \varepsilon_2\omega + \mathrm{i}\varepsilon_4\omega + \mathrm{i}\varepsilon_5\omega);\\
L_{24} &= \sqrt{P_1 P_2}(-B - \varepsilon_2\omega + \mathrm{i}\varepsilon_4\omega);\\
L_{31} &= \sqrt{P_1 P_2}(B - \varepsilon_2\omega);\\
L_{32} &= \sqrt{P_1 P_2}(B - \mathrm{i}\varepsilon_4\omega - \mathrm{i}\varepsilon_5\omega);\\
L_{33} &= P_2 + \Delta\omega + S_1\omega^2 - S_3\omega^4 - S_2\omega^3 \\
&\quad - \omega(2\varepsilon_1 P_2 + \varepsilon_2 P_1) - \mathrm{i}\omega(\varepsilon_3 P_2 + \varepsilon_5 P_1);\\
L_{34} &= P_2(1 - \varepsilon_1\omega - \mathrm{i}\varepsilon_3\omega);\\
L_{41} &= \sqrt{P_1 P_2}(-B - \varepsilon_2\omega + \mathrm{i}\varepsilon_4\omega + \mathrm{i}\varepsilon_5\omega);\\
L_{42} &= \sqrt{P_1 P_2}(-B - \varepsilon_2\omega);\\
L_{43} &= P_2(-1 - \varepsilon_1\omega + \mathrm{i}\varepsilon_3\omega);\\
L_{44} &= -P_2 + \Delta\omega - S_1\omega^2 + S_3\omega^4 - S_2\omega^3 \\
&\quad - \omega(2\varepsilon_1 P_2 + \varepsilon_2 P_1) + \mathrm{i}\omega(\varepsilon_3 P_2 + \varepsilon_5 P_1);
\end{aligned}$$

where $P_1 = 2P\cos^2(\phi)$ and $P_2 = 2P\sin^2(\phi)$, ϕ being the polarization angle. Now for achieving the MI condition required for the generation of ultrashort pulses of the order of 500 fs in the region of minimum group velocity dispersion, a similar procedure is followed as in case (i) of section 3 to arrive at the dispersion relation from equation (33) which is of the form

$$k = -S_2\omega^3 \pm \omega\sqrt{L_4 - 2\sqrt{L_5}}, \tag{40}$$

where L_4 and L_5 have the same form as obtained in section 3. Here, too, the condition for instability to occur is $L_4^2 < 4L_5$, as is clear from equation (40), and hence we obtain the same gain parameter as in case (i) of section 3 even though the eigenvalues are different in both cases. Hence all the results considered in case (i) of section 3 can be arrived at. Likewise, case (ii) presented in section 3 is analysed and we arrive numerically at the same results as obtained in section 3. Thus the modulational ansatz given by equation (37) can also effectively portray the MI phenomenon in the single-frequency propagation regime. Equation (38), being a linear homogenous ordinary differential equation, has a solution of the form

$$\mathbf{X}(\varsigma) = \exp(\mathrm{i}\mathbf{L}\varsigma)\mathbf{C}, \tag{41}$$

where the constant column matrix $\mathbf{C}$ depends on the initial conditions of the four linearized side band amplitudes. Figure 5 shows the spectrum for the side band amplitudes for various values of ς corresponding to the case (ii) in section 3 when equal power is distributed along both the axes (when the polarization angle $\phi = 45^\circ$). From the plots, we can infer three main results. The first is that MI can generate only one type of sideband on each fibre axis: an anti-Stokes sideband u_{a} (the solid curve in figure 5) on the fast axis and a Stokes sideband

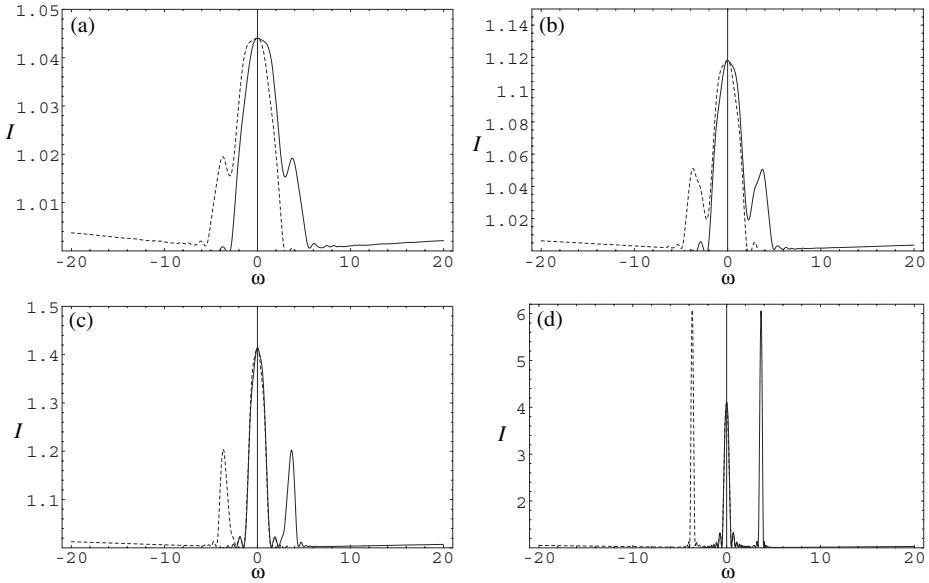

Figure 5. The intensities of the Stokes sideband amplitude represented by $|v_s(\omega)|^2$ (dashed curve) on the slow axis and the anti-Stokes side band amplitude represented by $|u_a(\omega)|^2$ (solid curve) on the fast axis for various values of ς corresponding to case (ii) in section 3: (a) $\varsigma = 0.6$; (b) $\varsigma = 0.8$; (c) $\varsigma = 2.0$; (d) $\varsigma = 8.0$. Also $I = |v_s|^2, |u_a|^2$.

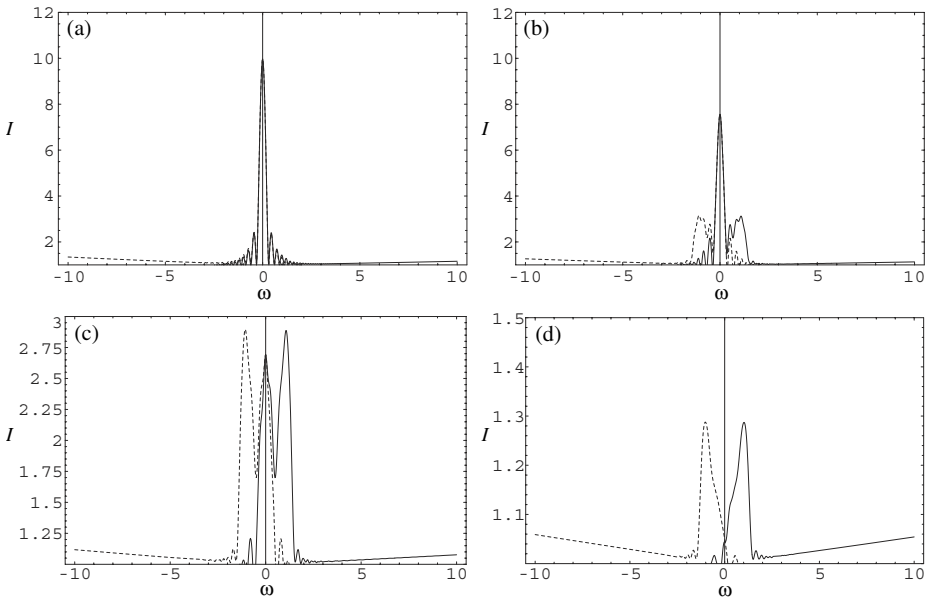

Figure 6. The intensities of the Stokes sideband amplitude represented by $|v_s(\omega)|^2$ (dashed curve) on the slow axis and the anti-Stokes side band amplitude represented by $|u_a(\omega)|^2$ (solid curve) on the fast axis for various values of unequal power distribution along both the axes corresponding to case (ii) in section 3: (a) $P_1 = 0.992$; $P_2 = 0.007$; (b) $P_1 = 0.75$; $P_2 = 0.25$; (c) $P_1 = 0.25$; $P_2 = 0.75$; (d) $P_1 = 0.03$; $P_2 = 0.97$. Also $I = |v_s|^2, |u_a|^2$.

v_s (the dashed curve in figure 5) on the slow axis. This has been experimentally observed by Millot *et al* [22]. u_a and v_s are called 'phase-matched waves' whereas u_s and v_a are called 'non phase-matched waves'. Also the intensity of the sidebands starts increasing as ς increases, and after some value of ς it becomes greater than the intensity of the mainband. This points to the fact that exchange of energy takes place between the spectral bands along the length of the fibre, which is our second result. From figure 5 we can decipher that for comparatively large values of ω, the spectrum increases linearly, which is due to the influence of SRS on the sideband spectrum. Until now we have considered equal power distribution along both the axes. Figure 6 depicts the spectrum for the sidebands for unequal power distribution along either axis corresponding to the case (ii) in section 3. From the plots it is clear that as P_1 decreases, with the total power $P = P_1 + P_2$ remaining a constant, the maximum value of the sideband amplitude decreases, which is our third result.

5. MI in a fibre Bragg grating

As has been discussed in the introduction, in this second part, we investigate MI in an FBG. We study the occurrence of MI

at the two edges (top and bottom) of the photonic bandgap (PBG) where the forward and backward propagating waves are strongly coupled because of the presence of the grating structure. We also study the MI when the continuous wave (cw) is detuned from the edges of the PBG into the anomalous and normal dispersion regimes.

MI in an FBG has been studied at two (low and high) power levels in an FBG for both anomalous- and normal-group velocity dispersion (GVD) regions, corresponding to upper and lower branches of the dispersion curves [39]. In the anomalous GVD case (upper branch), at relatively low powers ($\alpha < \kappa$), the gain spectrum is found to be similar to the case of a uniform index fibre. MI also occurs even in the normal GVD case (on the lower branch) where MI has a threshold condition. Thus, MI (in an FBG) on the lower branch is qualitatively different from the upper branch of the dispersion curves. In the former case, the instability has a finite threshold, meaning that the cws are stable. In other words, the cw fields are unstable only when the power of the cw fields exceeds the threshold condition [39]. In the latter case, the instability is thresholdless. Recently, MI has been observed experimentally in an apodized grating structure wherein which a single pulse has been converted into a train of ultrashort pulses [40, 41]. In addition to temporal instabilities, spatial temporal instabilities have also been studied in a nonlinear bulk medium with Bragg gratings in the presence of a Kerr-type nonlinearity [42]. More recently, there is a strong experimental evidence for the occurrence of MI in a FBG [43, 44].

Recently, fibre optic technology has advanced to the stage where it has become one of the most attractive solutions for reliable high speed and high capacity communication [1–3]. In particular, the regeneration and routing of information bearing optical signals in all-optical processing networks yield dramatic savings in power and cost [45]. Utilizing the speed and parallelism inherent to optics to the full extent, all optical signal processing elements (OPSE) have paved the way for overall bandwidth growth [46]. A main drawback for the OPSE is that they require devices that are uniformly stable for all incident intensities [47]. This requirement is met by passive optical limiters [48] which provide a uniformly stable operating regime, termed as true all-optical limiting, to a fairly good extent.

In a recent work, Pelinovsky *et al* have introduced the concept of nonlinearity management [49] of refractive optical gratings by suitably compensating Kerr nonlinearities leading to the disappearance of multistability resulting in hysteresis-free operation, and they have modelled a complete analytical theory [50] of true all-optical limiting in nonlinear optical gratings. Our present work concerns the study of the nonlinear continuous wave solution and its destabilization of the above-mentioned model by utilizing the concept of modulational instability. The MI phenomenon is accompanied by sideband evolution at a frequency separation from the carrier which is proportional to the optical pump power [51]. As regards applications, MI provides a natural means of generating ultrashort pulses at ultrahigh repetition rates, and it is thus potentially useful for the development of high speed optical communication systems in the future and hence has been exploited a great deal in many theoretical and experimental studies for the realization of laser sources adapted to ultrahigh bit-rate optical transmissions [52]. In our work, we concentrate on the MI conditions required for the generation of ultrashort pulses for the nonlinearity management system for both the anomalous and normal dispersion regimes.

6. Theoretical model

Pelinovsky *et al* have considered the coupled mode theory [49, 50] describing forward and backward propagating pulses for the nonlinearity management system pertaining to a Bragg grating. They have arrived at the nonlinear coupled mode (NLCM) equations [49, 50] that govern the nonlinear pulse propagation in a periodic nonlinear structure consisting of N alternating layers with different linear refractive indices and different Kerr nonlinearities having the form

$$\mathrm{i}\left(\frac{\partial A_\mathrm{f}}{\partial Z}+\frac{1}{v_\mathrm{g}}\frac{\partial A_\mathrm{f}}{\partial \tau}\right)+\delta A_\mathrm{f}+\kappa A_\mathrm{b}+\alpha\left(|A_\mathrm{f}|^2+2|A_\mathrm{b}|^2\right)A_\mathrm{f} + \beta[(2|A_\mathrm{f}|^2+|A_\mathrm{b}|^2)A_\mathrm{b}+A_\mathrm{f}^2A_\mathrm{b}^*]=0, \tag{42a}$$

$$-\mathrm{i}\left(\frac{\partial A_\mathrm{b}}{\partial Z}-\frac{1}{v_\mathrm{g}}\frac{\partial A_\mathrm{b}}{\partial \tau}\right)+\delta A_\mathrm{b}+\kappa A_\mathrm{f}+\alpha\left(|A_\mathrm{b}|^2+2|A_\mathrm{f}|^2\right)A_\mathrm{b} + \beta[(2|A_\mathrm{b}|^2+|A_\mathrm{f}|^2)A_\mathrm{f}+A_\mathrm{b}^2A_\mathrm{f}^*]=0, \tag{42b}$$

where Z and τ are the normalized spatial coordinate and time, respectively, and v_g is the group velocity far from the stop band associated with the grating. The parameters δ and κ are the detuning and linear coupling coefficients, respectively. The nonlinear terms in the time-domain coupled-mode equations contain contributions from both the self-phase modulation (SPM) and cross-phase modulation (XPM) effects. α and β are nonlinearity coefficients, β being the coefficient of nonlinearity management. The origin of the factor of 2 in the XPM coefficient has been discussed in detail in [1–3]. When $\beta = 0$, equations (42) reduce to the well known coupled-mode equations for the conventional FBG having positive Kerr coefficients along the propagation direction which has been studied extensively in the literature [53]. Equations (42) exhibit many interesting nonlinear effects. A modulational instability phenomenon throwing light on the possibility of the break-up of continuous or quasi-continuous waves into a train of ultrashort pulses is one such important nonlinear effect.

It has been well established that a knowledge of the nonlinear dispersion curves obtained from the continuous wave solutions of the coupled-mode equations can be used to understand the impact of nonlinearity on the photonic bandgap [3, 39]. Hence we assume continuous wave solutions for the basic equation, having the form [39]

$$A_\mathrm{f}=u_\mathrm{f}\exp(\mathrm{i}qZ), \qquad A_\mathrm{b}=u_\mathrm{b}\exp(\mathrm{i}qZ), \tag{43}$$

where u_f and u_b being the constants along the grating length are generally expressed in terms of a parameter $f=\frac{u_\mathrm{f}}{u_\mathrm{b}}$, which represents the ratio of forward- and backward-propagating waves. In other words, we can also say that the parameter f describes how the total power $P_0=u_\mathrm{f}^2+u_\mathrm{b}^2$ is divided between the forward- and backward-propagating waves and hence can be written as

$$u_\mathrm{f}=\sqrt{\frac{P_0}{1+f^2}}, \qquad u_\mathrm{b}=\sqrt{\frac{P_0}{1+f^2}}\,f. \tag{44}$$

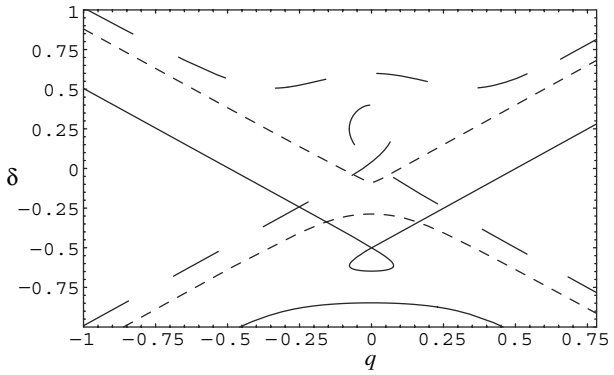

Figure 7. The dispersion curves traced by q and δ as f changes for various values of P_0 and β. On the upper branch of the figure, $f < 0$, whereas on the lower branch, $f > 0$. The solid curves ($\kappa = 0.1$, $P_0 = 2.0$, $\alpha = 0.5$ and $\beta = 0.001$) represent the dispersion curves for comparatively small values of the nonlinearity management coefficient β, and the dashed curves represent the same for large values of β ($\kappa = 0.1$, $P_0 = 2.0$, $\alpha = 0.5$ and $\beta = 0.5$). The dotted curve represents the linear case for which $\alpha = \beta = 0.0$.

f can be positive or negative. For values of $|f| < 1.0$, the backward wave dominates. On substituting equations (43) and (44) in the basic equation, the following dispersion relations are obtained:

$$q = -\kappa\frac{1-f^2}{2f} - \frac{\alpha P_0}{2}\frac{1-f^2}{1+f^2} - \frac{\beta P_0}{2}\frac{1-f^4}{1+f^2}, \qquad (45a)$$

$$\delta = -\kappa\frac{1+f^2}{2f} - \frac{3\alpha P_0}{2} - \frac{\beta P_0}{2f}\frac{f^4+6f^2+1}{1+f^2}. \qquad (45b)$$

When $\beta = 0$ in equation (45), the dispersion relations for the FBG case having the same positive Kerr coefficients [39] can be retrieved.

6.1. The role of nonlinearity on the PBG

In order to understand the role of nonlinearity on the PBG, we start our discussion from the low intensity (power) limit by setting α and β equal to zero. The dotted curve in figure 7 represents the dispersion curve for the linear case, in the low intensity limit, for both a uniform medium, represented as dashed lines, and a periodic medium, represented as solid curves. Note that the parameter q becomes purely imaginary when the frequency detuning δ of the incident light signal falls in the range $-\kappa < \delta < \kappa$. That is, the range $\delta \leqslant \kappa$ is referred to as the photonic bandgap (in analogy with the electronic energy bands occurring in crystals). For frequencies within the PBG, the grating reflectivity is high and the field envelopes are evanescent. However, for frequencies outside the PBG the grating reflectivity is lower (smaller). In other words, outside this PBG region, light can propagate inside the periodic structure. Therefore, for frequencies within the PBG, the grating does not allow running wave solutions, but for frequencies outside the PBG, travelling wave solutions are possible.

The parameter $f < 0$ represents (forward propagation) the upper branch of the dispersion curve where the grating-induced dispersion is negative (anomalous GVD). Similarly, the parameter $f > 0$ corresponds to (backward propagation) the lower branch of the dispersion curve where the grating-induced dispersion is positive (normal GVD). It is interesting to note that the parameter $f = \pm 1$ corresponds to the two edges of the photonic bandgap where the grating exhibits significant higher order dispersion [40]. The parameter $f = -1$ corresponds to tuning the cw beam to the top of the bandgap, and $f = 1$ corresponds to tuning the cw beam to the bottom of the bandgap. In this paper, we are interested in investigating the occurrence of MI at the edges of the PBG ($f = \pm 1$) as well as on the upper ($f < 0$) and lower ($f > 0$) branches of the dispersion curve. So far, we have discussed the concept of the photonic bandgap using the linear dispersion relation. In the forthcoming paragraph, we qualitatively discuss the impact of nonlinearity on the PBG.

The nonlinear dispersion relation can be used to describe the role of nonlinearity on the PBG structure. When we introduce positive (negative) nonlinearity into the system, it increases (decreases) the average refractive index of the medium, which in turn shifts the PBG such that the centre frequency does not fall within the frequency bandgap but corresponds to the allowed band. It also means that the high intensity electric field shifts the PBG (i.e., central frequency) to either of the upper or lower branches of the dispersion curves depending on the sign of nonlinearity. Thus positive nonlinearity shifts the PBG down in energy, and as a result the centre frequency now locally tunes out of the gap, i.e., to the upper edge of the PBG, whereas negative nonlinearity shifts the PBG up in energy, meaning that the central frequency is now shifted towards the higher frequency side (to the lower edge of the PBG). When the power of this applied electric field exceeds a certain, say, threshold power, i.e., critical power, the applied field drastically affects the PBG. Before embarking into further discussion, we first calculate the critical power. This critical value of P_0 can be calculated by looking for the value of f at which q becomes zero while $f \neq 1$ from the nonlinear dispersion relation, and it is found to be

$$f \equiv f_c = -\frac{\alpha P_0}{2(\kappa + \beta P_0)} \pm \sqrt{\left(\frac{\alpha P_0}{2(\kappa + \beta P_0)}\right)^2 - 1}. \qquad (46)$$

It is worth noting that when the nonlinear (negative) Kerr coefficient is zero, the above result leads to the already predicted result for the standard NLCM equations.

Figure 7 portrays the dispersion curves traced by q and δ as f changes for various values of P_0 and β. On the upper branch of figure 7, $f < 0$, whereas on the lower branch, $f > 0$. The two edges of the stop band occur at $f = \pm 1.0$. Equation (45) throws light on the effect of fibre nonlinearity on the dispersion curves. For example, for comparatively small values of the nonlinearity management coefficient β, on changing the values of the input power P_0 beyond a critical value, the upper branch of the dispersion curve changes qualitatively, leading to the formation of a loop (the solid curves in figure 7). But for comparatively large values of β, the lower branch of the dispersion curve forms a loop while the upper branch develops a double well parabolic form (the dashed curves in figure 7). This behaviour shows that both the branches of the dispersion curves are placed at two different power levels.

6.2. Linear stability analysis

Extensive research has been carried out in studying the MI phenomenon [3, 39–43] by which the steady-state solution

is destabilized, producing periodic output even when a continuous wave is incident on one end of the fibre grating. The pulse trains so generated via MI have the added advantage of being tuned over a large range because of large group velocity dispersion changes occurring with the detuning δ [40]. Hence, in this work, we perturb the steady-state solutions, given by equation (43), slightly without imposing boundary conditions at the grating ends, as

$$A_j = (u_j + a_j)\exp(\mathrm{i}qZ), \qquad (j = \mathrm{f}, \mathrm{b}), \tag{47}$$

in order to study the effect of nonlinearity management on MI. The fundamental idea of linear stability analysis (LSA) is to perturb the (system under consideration) continuous wave (cw) solution slightly and then study whether this small perturbation grows or decays with propagation. It should be emphasized that LSA is valid as long as the perturbation amplitude remains small compared with the cw beam amplitude. In the case when the perturbation amplitude grows enough, and if it is comparable to that of the incident cw beam, then numerical analysis must be adopted. In this paper, we restrict ourselves to the former case. Assuming that the perturbation a_j is small, we substitute equation (47) into the basic equations and linearize in a_j to obtain

$$\begin{aligned}\mathrm{i}\left(\frac{\partial a_\mathrm{f}}{\partial Z} + \frac{1}{v_\mathrm{g}}\frac{\partial a_\mathrm{f}}{\partial \tau}\right) - \kappa f a_\mathrm{f} + \kappa a_\mathrm{b} + \frac{\alpha P_0}{1+f^2}\left[a_\mathrm{f} + a_\mathrm{f}^*\right.\\ \left. + 2f\left(a_\mathrm{b} + a_\mathrm{b}^*\right)\right] + \frac{\beta P_0}{1+f^2}\left[2a_\mathrm{b} + a_\mathrm{b}^* + f\left(a_\mathrm{f} + 2a_\mathrm{f}^*\right)\right.\\ \left. + f^2\left(2a_\mathrm{b} + a_\mathrm{b}^*\right) - f^3 a_\mathrm{b}\right] = 0, \end{aligned} \tag{48a}$$

$$\begin{aligned}-\mathrm{i}\left(\frac{\partial a_\mathrm{b}}{\partial Z} - \frac{1}{v_\mathrm{g}}\frac{\partial a_\mathrm{b}}{\partial \tau}\right) - \frac{\kappa}{f}a_\mathrm{b} + \kappa a_\mathrm{f} + \frac{\alpha P_0}{1+f^2}\left[2f\left(a_\mathrm{f} + a_\mathrm{f}^*\right)\right.\\ \left. + f^2\left(a_\mathrm{b} + a_\mathrm{b}^*\right)\right] + \frac{\beta P_0}{1+f^2}\left[2a_\mathrm{f} + a_\mathrm{f}^* + f\left(a_\mathrm{b} + 2a_\mathrm{b}^*\right)\right.\\ \left. + f^2\left(2a_\mathrm{f} + a_\mathrm{f}^*\right) - \frac{a_\mathrm{b}}{f}\right] = 0. \end{aligned} \tag{48b}$$

In order to solve the set of two linearized equations given by equation (48), we assume a plane wave ansatz, constituted of both forward and backward propagation, having the form [3, 39]

$$a_j = c_j\exp(\mathrm{i}(KZ - \Omega\tau)) + d_j\exp(-\mathrm{i}(KZ - \Omega\tau)), \quad (j = \mathrm{f}, \mathrm{b}), \tag{49}$$

where c_j and d_j are real constants, K the propagation constant and Ω the perturbation frequency. Following the method discussed in [39], on substituting equation (49) into (48), we obtain a set of four homogeneous equations satisfied by c_j and d_j. This set has a nontrivial solution only when the 4×4 determinant formed by the coefficients matrix vanishes as given below:

$$\begin{vmatrix} m_{11} & m_{12} & m_{13} & m_{14} \\ m_{21} & m_{22} & m_{23} & m_{24} \\ m_{31} & m_{32} & m_{33} & m_{34} \\ m_{41} & m_{42} & m_{43} & m_{44} \end{vmatrix} = 0, \tag{50}$$

where

$$m_{11} = -K + s - \kappa f + \Gamma_1 + \Gamma_2 f(1 - f^2),$$

$$m_{12} = \kappa + 2\Gamma_1 f + 2\Gamma_2(1 + f^2),$$

$$m_{13} = \Gamma_1 + 2\Gamma_2 f,$$

$$m_{14} = 2\Gamma_1 f + \Gamma_2(2 + f^2),$$

$$m_{21} = m_{12},$$

$$m_{22} = K + s - \frac{\kappa}{f} + \Gamma_1 f^2 - \frac{\Gamma_2}{f} + \Gamma_2 f,$$

$$m_{23} = 2\Gamma_1 f + \Gamma_2(1 + f^2),$$

$$m_{24} = \Gamma_1 f^2 + 2\Gamma_2 f,$$

$$m_{31} = m_{13},$$

$$m_{32} = m_{23},$$

$$m_{33} = K - s - \kappa f + \Gamma_1 + \Gamma_2 f(1 - f^2),$$

$$m_{34} = m_{12},$$

$$m_{41} = m_{23},$$

$$m_{42} = m_{24},$$

$$m_{43} = m_{12},$$

$$m_{44} = -K - s - \frac{\kappa}{f} + \Gamma_1 f^2 - \frac{\Gamma_2}{f} + \Gamma_2 f.$$

This condition leads to a fourth order polynomial in $s \equiv \frac{\Omega}{v_\mathrm{g}}$ whose roots depend on K, κ and P_0. The four roots of the polynomial in s so obtained determine the stability of the continuous wave solution.

As is well known, for the case of a FBG, MI occurs when there is an exponential growth in the amplitude of the perturbed wave, which implies the existence of a nonvanishing imaginary part in the complex parameter s [3, 39]. The MI phenomenon is measured by a gain given by $G \equiv |\mathrm{Im}\, s_m|$, where $\mathrm{Im}\, s_m$ denotes the imaginary part of s_m, where s_m is the root with the largest imaginary part.

In this second part of the paper, our aim is to investigate the occurrence of temporal (longitudinal) instabilities of two counterpropagating waves in an FBG structure at the edges of the bandgap as well as on the upper and lower branches of the dispersion curve. The results of this paper are presented in the following subsections. First we study the MI for the general case (where $f < 0$ and $f > 0$) and then consider the two more special cases where $f = \pm 1$.

6.3. The anomalous dispersion regime ($f < 0$)

First we consider the general case where the parameter $f < 0$ describes the detuning of the cw from the edge of the PBG into the anomalous dispersion regime (upper branch of the dispersion curve). We obtain the gain spectra of MI for both the anomalous and normal dispersion regimes for two cases (a) gain, $G(K, \kappa) \equiv |\mathrm{Im}\, s_m(K, \kappa)|$ for a particular value of the input power P_0, and (b) $G(K, P_0) \equiv |\mathrm{Im}\, s_m(K, P_0)|$

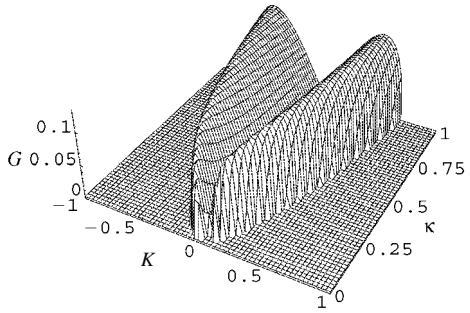

Figure 8. Gain spectrum in the anomalous dispersion regime, for the following physical parameters: $P_0 = 0.1$, $\beta = 0.001$, $\alpha = 0.5$ and $f = -0.5$.

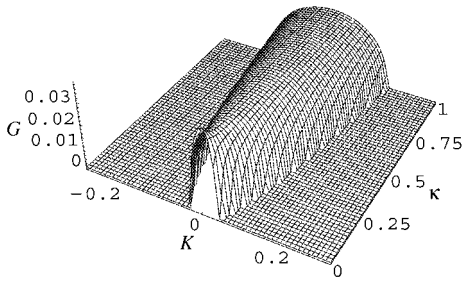

Figure 9. Gain spectrum in the anomalous dispersion regime, for the following physical parameters: $P_0 = 0.1$, $\beta = 0.5$, $\alpha = 0.5$ and $f = -0.5$.

for a particular value of the linear coupling constant κ. We summarize the results obtained below. For the first case, in the anomalous dispersion regime, for comparatively small values of the input power $P_0 = 0.1$ and nonlinearity management coefficient $\beta = 0.001$, we obtain the gain spectrum having two distinct sidelobes on either side of zero propagation constant region and with nil value along the line where the propagation constant vanishes. Also, the sidelobes broaden with increasing height as the value of the linear coupling coefficient κ increases. This is depicted in figure 8. For the same situation, but having comparatively large value of the nonlinearity management coefficient, say $\beta = 0.5$, the sidelobes vanish and, instead, we obtain a gain spectrum centred around the zero propagation constant region and having a maximum value along the line where the propagation constant vanishes. Also, the centred lobe broadens with increasing κ, as is portrayed in the surface plot given by figure 9. This is one of our main results.

6.4. The top of the photonic bandgap ($f = -1$)

So far, we have considered the case for which $f = -0.5$. It is well known that the parameter $f = -1$ represents the tuning of the cw into the top of the photonic bandgap. Now on repeating the same procedure for $f = -1.0$, in addition to having a centred lobe, we observe two distinct curves whose heights reduce and soon become zero with increasing κ, on either side of the zero propagation constant.

6.5. The normal dispersion regime ($f > 0$)

Again we consider the other general case for which the parameter $f > 0$, which represents the detuning of the

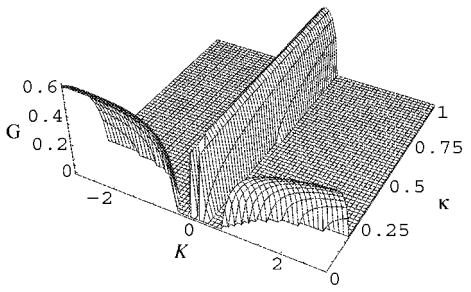

Figure 10. Gain spectrum in the anomalous dispersion regime, for the following physical parameters: $P_0 = 0.5$, $\beta = 0.9$, $\alpha = 0.5$ and $f = -1.0$.

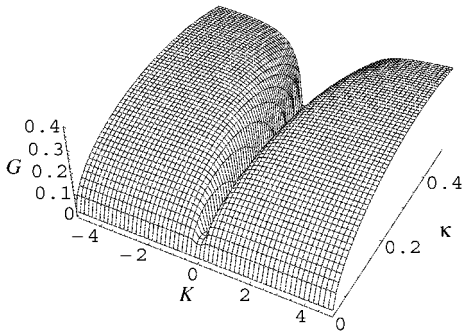

Figure 11. Gain spectrum in the normal dispersion regime, for the following physical parameters: $P_0 = 0.5$, $\beta = 0.001$, $\alpha = 0.5$ and $f = 0.5$.

cw into the lower branch of the dispersion curve where the grating-induced dispersion is normal (positive). For the normal dispersion regime, for $P_0 = f = 0.5$ and for comparatively small values of the nonlinearity management coefficient, say $\beta = 0.001$, the gain spectrum has values expected along the line where the propagation constant vanishes for which it has nil value. Figure 10 portrays the corresponding surface plot. Now, for comparatively large values of the nonlinearity management coefficient, say $\beta = 0.5$, the gain spectrum has a 'w' shaped form centred around the zero propagation constant region and with the edges being flattened, as depicted in figure 11.

6.6. The bottom of the photonic bandgap ($f = 1$)

As discussed earlier, $f = 1$ corresponds to tuning the cw beam to the bottom of the photonic bandgap. On repeating the same procedure for $f = 1.0$, which depicts tuning at the bottom of PBG, for comparatively small values of the NMC, say $\beta = 0.001$, the gain spectrum has nil value along the zero propagation constant region but has maximum values along the line where the propagation constant vanishes for comparatively large values of the NMC, say $\beta = 0.5$, as is portrayed in figure 12. So far, we have plotted the gain spectrum by varying the linear coupling constant κ and keeping the input power P_0 fixed. Now on keeping the linear coupling constant κ fixed and on varying the input power P_0, we observe that the MI condition is achieved for comparatively small values of P_0 for both the anomalous and normal dispersion regimes, which is our main result, contrary to that of the birefringent fibre case where large values of the input power are required [30]. This is

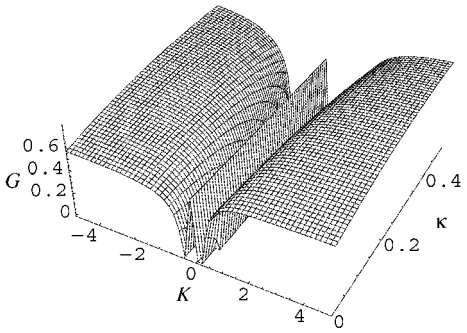

Figure 12. Gain spectrum in the normal dispersion regime for the following physical parameters: $P_0 = 0.5, \beta = 0.5, \alpha = 0.5$ and $f = 0.5$.

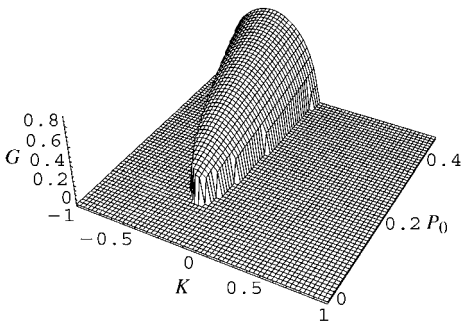

Figure 13. Gain spectrum in the anomalous dispersion regime for various values of the input power P_0 and for the following physical parameters: $\beta = 0.1, \alpha = 1.4, \kappa = 0.2$, and $f = -0.5$.

depicted in the surface plots given by figures 13 and 14. From the figures, we observe that MI condition is achieved only for finite values of the input power.

Having discussed the MI gain spectra for both anomalous and normal dispersion regimes in the upper and lower branches of the dispersion curve for the nonlinearity management system, in the following section we argue the existence of the soliton in the upper and lower branches of the dispersion curve through the same physical parameter values for which the MI gain spectra have already been obtained.

7. Discussion on the existence of the gap soliton

As discussed above, here, our prime aim is to discuss the generation of solitons for the nonlinearity management system in the upper and lower branches of the dispersion curve through the MI gain spectra.

Like a conventional soliton in a uniform fibre, the soliton in a FBG is formed through a delicate balance between the Kerr nonlinearity and the strong GVD exhibited by the PBG structure. The resulting solitons are often referred to as Bragg grating solitons on account of the fact that they are formed within the FBG. When the entire spectral components of the input pulse lie within the PBG structure, the pulse gets completely reflected as solitons which result from the counterbalancing effects of self-and cross-phase modulations with the grating-induced dispersion. The resulting solitons are referred to as gap solitons, since their spectral components are within the PBG structure. However, it can be noticed that, in literatures, nowadays the distinction between gap solitons and

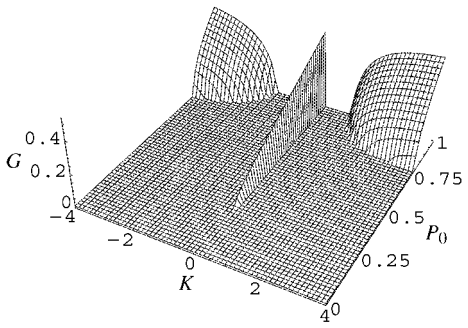

Figure 14. Gain spectrum in the normal dispersion regime for various values of the input power P_0 and for the following physical parameters: $\beta = 0.1, \alpha = 1.4, \kappa = 0.2$, and $f = 0.5$.

Bragg grating solitons is hardly maintained and, in general, they are simply called grating solitons. These solitons have been extensively investigated by many research groups [53–60] in the FBG, and still the investigations on these exciting entities are alive. For instance, Chen and Mills [54] were the first to predict the existence of self-localization of a light wave within the PBG of a nonlinear grating and they coined the name gap soliton.

To investigate these solitons in the FBG, so far, two theoretical approaches have been developed. The first one is the coupled mode theory, which describes a coupling between forward and backward travelling modes where the nonlinear pulse propagation is described by the NLCM equations. In general, the NLCM equations are nonintegrable and are applicable anywhere in the PBG structure. However, in a few cases, NLCM equations have analytical solutions representing the solitary wave solutions. The most general form of the solitary wave solutions to the NLCM equations with β being zero were derived, for the first time, by Aceves and Wabnitz [57]. They are given by

$$A_{\pm} = \mu \tilde{A}_{\pm} \exp[i\eta(\theta)]$$
$$\tilde{A}_{+} = \mp\sqrt{\frac{\pm\kappa}{2}}\frac{1}{\Delta}\sin\tilde{\delta}\exp(\pm i\sigma)\,\mathrm{sech}\left(\theta \pm \frac{i\tilde{\delta}}{2}\right) \qquad (51)$$
$$\tilde{A}_{-} = -\sqrt{\frac{\pm\kappa}{2}}\Delta\sin\tilde{\delta}\exp(\pm i\sigma)\,\mathrm{sech}\left(\theta \pm \frac{i\tilde{\delta}}{2}\right)$$

with

$$\theta = \kappa\gamma(\sin\tilde{\delta})(z - vt),\ \sigma = \kappa\gamma(\cos\tilde{\delta})(vz - t),$$
$$v = \frac{1-\Delta^4}{1+\Delta^4}\gamma = \frac{1}{\sqrt{1-v^2}}.$$

In equation (51), γ is the Lorentz factor. Since the expressions for μ and η are well known, we do not present them here. The soliton-like solutions for the NLCM equations are considered to be a generalization of the massive thirring model (MTM). As a special case, when $\tilde{\delta} = \pi/2$, the most general solutions of Aceves and Wabnitz lead to the slow Bragg solitons, already predicted by Christodoulides and Joseph [56].

The second one is the Bloch wave analysis, which is used to describe the nonlinear pulse propagation near the PBG structure. To achieve the same, usually a technique known as multiple scale analysis is adopted. Recently, using the multiple analysis, Aceves [58] investigated the gap soliton bullets in

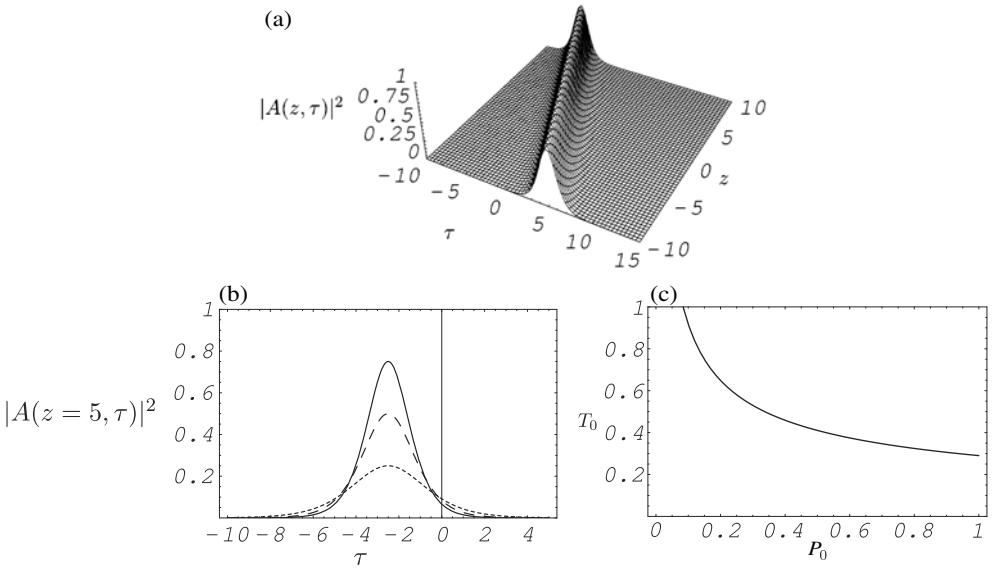

Figure 15. Bright soliton solution in the upper branch of the dispersion curve given by equation (52): (a) surface plot for the intensity of the bright soliton having the following values for the physical parameters: $P_0 = 0.5$, $\alpha = 1.4$, $\beta = 0.1$, $\beta_1 = 0.5$ and $\kappa = 0.2$; (b) intensity plot for various values of input power: $P_0 = 0.25$ (dotted curve), $P_0 = 0.5$ (dashed curve) and $P_0 = 0.75$ (solid curve); (c) variation of pulse width T_0 with respect to the input power P_0 given by the expression $T_0 = \sqrt{\frac{2}{dP_0}}$, which is obtained from equation (53).

the Kerr-type planar waveguides. Very recently, following the same multiple scale analysis, we have investigated bright and dark solitons in the FBG [60].

At this juncture, we would like to show the generation of bright and dark solitons in the upper and lower branches of the dispersion curve through the MI gain spectra scheme. Note that the formation of these solitons depends on the critical power of the MI gain spectra. From the MI gain spectrum of figure 13, we find that the critical power (P_c) is less than 0.2. Therefore, the bright soliton is formed in the upper branch (AD regime) for the input power $P_0 > 0.2$.

$$A(z,\tau) = \sqrt{P_0}\,\mathrm{sech}\left[\frac{1}{T_0\sqrt{b}}(\tau+\beta_1 z)\right]\exp[\mathrm{i}(kz-\omega\tau)], \quad (52)$$

where

$$P_0 = 2\left(\frac{2a\omega+3b\omega^2-\beta_1}{d}\right), \qquad T_0 = \sqrt{\frac{1}{2a\omega+3b\omega^2-\beta_1}}. \quad (53)$$

It should be noted that the coefficients $a = \frac{1}{2\kappa}$, $b = \frac{1}{8\kappa^3}$ and $d = \frac{3\alpha-4\beta}{4\kappa^2}$ are the physical parameters of the above NLCM equations. The parameter ω is the frequency and β_1 is the group velocity. In equation (52), the variable 'A' represents the amplitude of the envelope associated with the Bloch wave formed by a superposition of forward A_f and backward A_b propagating waves [1, 4]. The bright soliton is depicted in figure 15(a). Further, to have an idea about the variation of pulse width and amplitude with respect to input power P_0, we have also provided the 2D plots for various values of the input power P_0. From the plot, it is clear that the pulse width reduces and hence the amplitude increases as the value of the input power P_0 increases. This is clearly depicted in figure 15(b). In addition, we have found the relation connection between input power P_0 and pulse width T_0 which is clearly shown in figure 15(c).

Similarly, there is another interesting class of soliton, called a dark soliton, in the lower branch; now we discuss the generation of the same. To do so, we observe the critical power from the MI gain spectrum of the normal dispersion regime, and it is found to be of the order of 0.25 from figure 14. Hence the dark soliton is formed in the lower branch for $P_0 > 0.25$. The dark soliton solution is

$$A(z,\tau) = \sqrt{P_0}\tanh\left[\frac{1}{T_0\sqrt{b}}(\tau+\beta_1 z)\right]\exp[\mathrm{i}(kz-\omega\tau)], \quad (54)$$

where

$$P_0 = \frac{2a\omega+3b\omega^2-\beta_1}{d}, \qquad T_0 = \sqrt{\frac{2}{2a\omega+3b\omega^2-\beta_1}}. \quad (55)$$

The dark soliton in the lower branch is depicted in figure 16(a). In addition, we have also provided the 2D plots for various values of the critical power. From the plot, it is clear that the pulse width reduces and hence the amplitude increases as the value of input power P_0 increases, as in the case of the bright soliton. This is clearly depicted in figure 16(b).

8. Conclusion

The conditions for the occurrence of cross-phase MI in the normal dispersion regime which occurs as a result of a group velocity mismatch between the linearly polarized eigenstates when the linearly polarized pump is oriented at 45° with respect to the slow or fast axis are obtained. The instability conditions that govern the generation of ultrashort pulses for the two cases mentioned in section 3 are not affected irrespective of the presence or absence of S_2, the dimensionless

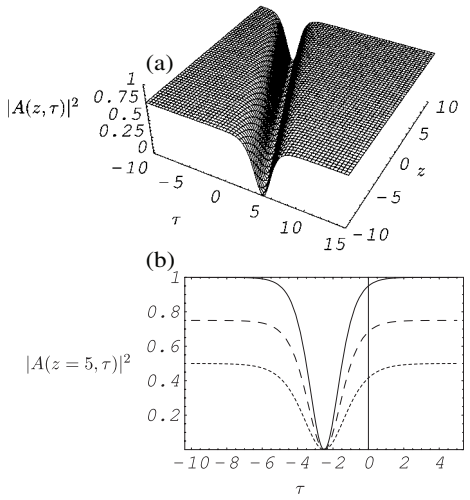

Figure 16. Dark soliton solution in the lower branch of the dispersion curve given by equation (54): (a) surface plot for the intensity of the dark soliton having the same physical parameter values as in the bright soliton case; (b) intensity plot for various values of input power: $P_0 = 0.5$ (dotted curve), $P_0 = 0.75$ (dashed curve) and $P_0 = 1.0$ (solid curve).

third order dispersion coefficient. For variations in the pump polarization, maximum gain occurs for 45° polarization for all the cases considered in this paper. The effect of SRS on MI is such that for comparatively small values of the perturbation frequency, group velocity dispersion and cross-phase modulation terms dominate, whereas for comparatively large values of the perturbation frequency the gain spectrum increases linearly, with the result that the region of MI is widened due to SRS. Moreover, the self-steepening effect reduces the maximum gain and bandwidth. At the zero group velocity dispersion regime, one obtains only the original MI. Furthermore, a modulational ansatz given by equation (37) for the perturbation amplitudes is considered, and we observe that

(i) MI can generate only one type of sideband on each fibre axis: an anti-Stokes sideband u_a on the fast axis and a Stokes sideband v_s on the slow axis;
(ii) the intensity of the sidebands starts increasing as ς increases and after some value of ς becomes greater than the intensity of the mainband, which points to the fact that exchange of energy takes place between the spectral bands along the length of the fibre;
(iii) for unequal power distribution along either axis, the maximum value of the sideband decreases as P_1 decreases with the total power $P = P_1 + P_2$ remaining a constant.

In addition to the investigation of MI in fibres, we have also investigated the modulational instability conditions required for the generation of ultrashort pulses in FBG for the nonlinearity management system for both the anomalous and normal dispersion regimes as well as at the edges of the photonic bandgap, and have arrived at two main results. One is that modulational instability occurs only for finite values of the total input power for both the anomalous and normal dispersion regimes. The other is that the gain spectrum changes profusely for comparatively smaller and comparatively larger values of the nonlinearity dispersion management coefficient. Through the nonlinear dispersion curves, we have qualitatively studied the impact of nonlinearity on the photonic bandgap. From the results, it is clear that the top of the photonic bandgap is drastically affected by the positive nonlinearity whenever the power of the applied field exceeded the critical power. We have also discussed the generation of bright and dark solitons in an FBG derived from the various MI gain spectra scheme discussed in section 6. We have found that there exists a relation between the total input power and the soliton pulse width, and observed that on increasing the total input power, the soliton pulse amplitude increases for both the anomalous and normal dispersion regimes and also gets compressed. Here, our studies have been restricted to only temporal instabilities of two counterpropagating waves. Therefore, it would be of great interest to extend the above analysis to both longitudinal and transverse instabilities (called spatiotemporal instability) in a bulk medium having the grating structure. Another important study is the impact of dissipation on the modulational instability gain spectrum, which should ultimately result in a decrease of the gain along the length of the fibre Bragg grating, which is under study.

Acknowledgments

KP wishes to thank DST, UGC (Research Award) and CSIR, Government of India, for financial support through research projects. KSN wishes to acknowledge CSIR for the award of a SRF.

References

[1] Kivshar Y S and Agrawal G P 2003 *Optical Solitons—From Fibers to Photonic Crystals* (San Diego, CA: Academic)
[2] Hasegawa A 2003 *Optical Solitons—Theoretical and Experimental Challenges* vol 613, ed K Porsezian and V C Kuriakose (Berlin: Springer)
[3] Agrawal G P 2001 *Nonlinear Fiber Optics* (San Diego, CA: Academic)
[4] Agrawal G P 2001 *Applications of Nonlinear Fiber Optics* (San Diego, CA: Academic)
[5] Akhmediev N N and Ankiewicz A 1997 *Solitons–Nonlinear Pulses and Beams* (London: Chapman and Hall)
[6] Hasegawa A and Kodama Y 1995 *Solitons in Optical Communications* (Oxford: Clarendon)
[7] Tai K, Hasegawa A and Tomita A 1986 *Phys. Rev. Lett.* **56** 135
[8] Berkhoer A L and Zakharov V E 1970 *Sov. Phys.—JETP* **31** 486
[9] Rothenberg J E 1990 *Phys. Rev.* A **42** 682
[10] Drummond P D, Kennedy T A B, Dudley J M, Leonhardt R and Harvey J D 1990 *Opt. Commun.* **78** 137
[11] Millot G, Pitois S, Seve E, Dinda P T, Grelu P, Wabnitz S, Haelterman M and Trillo S 1999 *Optical Solitons: Theoretical Challenges and Industrial Perspectives* ed V E Zakharov and S Wabnitz (France: Springer)
[12] Ostrovskii L A 1966 *Sov. Phys.—JETP* **24** 797
[13] Karpman V I 1967 *JETP Lett.* **6** 277
[14] Hasegawa A 1970 *Phys. Rev. Lett.* **24** 1165
[15] Hasegawa A and Brinkman W F 1980 *IEEE J. Quantum Electron.* **16** 694
[16] Seve E, Dinda P T, Millot G, Remoissenet M, Bilbault J M and Haelterman M 1996 *Phys. Rev.* A **54** 3519
[17] Millot G, Seve E and Wabnitz S 1997 *Phys. Rev. Lett.* **79** 661
[18] Millot G, Seve E and Wabnitz S 1998 *Phys. Rev. Lett.* **80** 504
[19] Pitois S, Millot G and Wabnitz S 1998 *Phys. Rev. Lett.* **81** 1409
[20] Pitois S, Millot G, Grelu P and Haelterman M 1999 *Phys. Rev.* A **60** 994
[21] Millot G, Dinda P T, Seve E and Wabnitz S 2001 *Opt. Fiber Technol.* **7** 170

[22] Millot G, Pitois S, Dudley J M and Haelterman M 2003 *Optical Solitons—Theoretical and Experimental Challenges* vol 613, ed K Porsezian and V C Kuriakose (Berlin: Springer)
[23] Greer E J, Patrick D M and Wigley P G J 1989 *Electron. Lett.* **25** 1246
[24] Yu M, McKinistric C J and Agrawal G P 1998 *J. Opt. Soc. Am.* B **15** 607
[25] Steel M J, White T P and de Sterke C M 2001 *Opt. Lett.* **26** 488
[26] Seve E, Dinda P T, Millot G, Remoissenet M, Bilbault J M and Haelterman M 1996 *Phys. Rev.* A **54** 3519
[27] Dudley J M, Thomson M D, Gutty F, Pitois S, Grelu P and Millot G 1999 *Electron. Lett.* **35** 2042
[28] Pitois S, Haelterman M and Millot G 2002 *J. Opt. Soc. Am.* B **19** 782
[29] Drummond P D, Kennedy T A B and Harvey J D 1990 *Opt. Commun.* **78** 137
[30] Ganapathy R and Kuriakose V C 2002 *Pramana J. Phys.* **58** 668
[31] Eggleton B J, Slusher R E, de Sterke C M, Krug P A and Sipe J E 1996 *Phys. Rev. Lett.* **76** 1627
[32] Malomed B A and Tasgal R A 1996 *J. Nonlinear Opt. Phys. Mater.* **5** 559
[33] Malomed B A and Tasgal R A 1996 *Pure Appl. Opt.* **5** 947
[34] Menyuk C R 1989 *IEEE J. Quantum Electron.* **25** 2674
[35] Cavalcanti S B, Cressoni J C, da Cruz H R and Gouveia-Neto A S 1991 *Phys. Rev.* A **43** 6162
[36] Buryak A V and Akhmediev N N 1995 *Phys. Rev.* E **51** 3572
[37] Akhmediev N N, Buryak A V and Soto-Crespo J M 1994 *Opt. Commun.* **112** 278
[38] Xu W-C, Zhang S-M, Chen W-C, Luo A-P and Liu S-H 2001 *Opt. Commun.* **199** 355
[39] de Sterke C M 1998 *J. Opt. Soc. Am.* B **15** 2660
[40] Eggleton B J, de Sterke C M and Slusher R E 1997 *J. Opt. Soc. Am.* B **14** 2980
[41] Eggleton B J, de Sterke C M, Aceves A B, Sipe J E, Strasser T A and Slusher R E 1998 *Opt. Commun.* **149** 267
[42] Litchinitser N M, McKinstrie C J, de Sterke C M and Agrawal G P 2001 *J. Opt. Soc. Am.* B **18** 45
[43] Pitois S, Haelterman M and Millot G 2001 *Opt. Lett.* **26** 780
[44] Pitois S, Haelterman M and Millot G 2002 *J. Opt. Soc. Am.* B **19** 782
[45] Tran P 1999 *J. Opt. Soc. Am.* B **16** 70
[46] Smith P W E and Qian L 1999 *Circ. Devices* **15** 28
[47] He J and Cada M 1991 *IEEE J. Quantum Electron.* **27** 1182
[48] Brzozowski L and Sargent E H 2000 *IEEE J. Quantum Electron.* **36** 550
[49] Pelinovsky D, Brzozowski L and Sargent E H 2000 *Phys. Rev.* E **62** R4536
[50] Pelinovsky D, Sears J, Brzozowski L and Sargent E H 2002 *J. Opt. Soc. Am.* B **19** 43
[51] Seve D E, Dinda P T, Millot G, Remoissenet M, Bilbault J M and Haelterman M 1996 *Phys. Rev.* A **54** 3519
[52] Steel M J, White T P and de Sterke C M 2001 *Opt. Lett.* **26** 488
[53] de Sterke C M and Sipe J E 1994 *Progress in Optics* vol 33, ed E Wolf (Amsterdam: Elsevier)
[54] Chen W and Mills D L 1987 *Phys. Rev. Lett.* **58** 160
[55] Sipe J E and Winful H G 1988 *Opt. Lett.* **13** 132
[56] Christodoulides D N and Joseph R I 1989 *Phys. Rev. Lett.* **62** 1746
[57] Aceves A B and Wabnitz S 1989 *Phys. Lett.* A **141** 37
[58] Aceves A B 2003 *Optical Solitons: Theoretical and Experimental Challenges* (*Springer Lecture Notes in Physics* vol 613) ed K Porsezian and V C Kuriakose (Berlin: Springer)
[59] Senthilnathan K, Porsezian K and Malathi P 2003 *J. Opt. Soc. Am.* B **20** 366
[60] Senthilnathan K, Porsezian K, Ramesh Babu P and Santhanam V 2003 *IEEE J. Quantum Electron.* **39** 1492